THE JOURNAL OF PHYSICAL CHEMISTRY A

Article

pubs.acs.org/JPCA

Isomeric Product Detection in the Heterogeneous Reaction of Hydroxyl Radicals with Aerosol Composed of Branched and Linear Unsaturated Organic Molecules

Theodora Nah,[†,‡] Haofei Zhang,[‡,§] David R. Worton,[§,∥] Christopher R. Ruehl,[‡] Benjamin B. Kirk,[‡] Allen H. Goldstein,[§,⊥,#] Stephen R. Leone,[†,‡,○] and Kevin R. Wilson*[,‡]

[†]Department of Chemistry, [§]Department of Environmental Science, Policy, and Management, [#]Department of Civil and Environmental Engineering, and [○]Department of Physics, University of California, Berkeley, California 94720, United States

[‡]Chemical Sciences Division and [⊥]Environmental and Energy Technologies Division, Lawrence Berkeley National Laboratory, Berkeley, California 94720, United States

[∥]Aerosol Dynamics Inc., Berkeley, California 94710, United States

Supporting Information

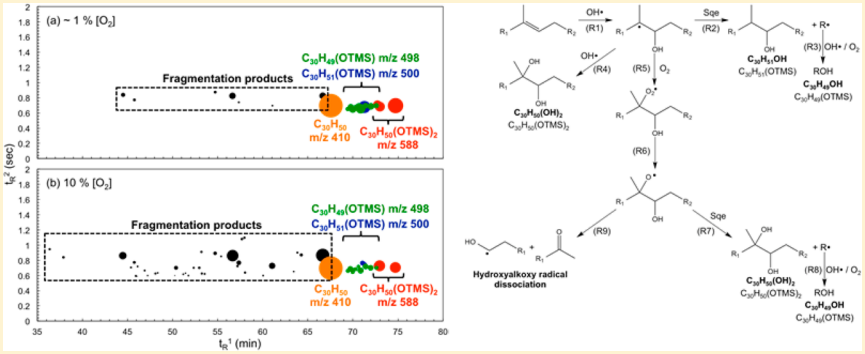

ABSTRACT: The influence of molecular structure (branched vs linear) on product formation in the heterogeneous oxidation of unsaturated organic aerosol is investigated. Particle phase product isomers formed from the reaction of squalene ($C_{30}H_{50}$, a branched alkene with six C=C double bonds) and linolenic acid ($C_{18}H_{30}O_2$, a linear carboxylic acid with three C=C double bonds) with OH radicals are identified and quantified using two-dimensional gas chromatography−mass spectrometry. The reactions are measured at low and high $[O_2]$ (~1% vs 10% $[O_2]$) to understand the roles of hydroxyalkyl and hydroxyperoxy radical intermediates in product formation. A key reaction step is OH addition to a C=C double bond to form a hydroxyalkyl radical. In addition, allylic alkyl radicals, formed from H atom abstraction reactions by hydroxyalkyl or OH radicals play important roles in the chemistry of product formation. Functionalization products dominate the squalene reaction at ~1% $[O_2]$, with the total abundance of observed functionalization products being approximately equal to the fragmentation products at 10% $[O_2]$. The large abundance of squalene fragmentation products at 10% $[O_2]$ is attributed to the formation and dissociation of tertiary hydroxyalkoxy radical intermediates. For linolenic acid aerosol, the formation of functionalization products dominates the reaction at both ~1% and 10% $[O_2]$, suggesting that the formation and dissociation of secondary hydroxyalkoxy radicals are minor reaction channels for linear molecules. The distribution of linolenic acid functionalization products depends upon $[O_2]$, indicating that O_2 controls the reaction pathways of the secondary hydroxyalkyl radical. For both reactions, alcohols are formed in favor of carbonyl functional groups, suggesting that there are some key differences between heterogeneous reactions involving allylic radical intermediates and those reactions of OH radicals with simple saturated hydrocarbons.

1. INTRODUCTION

The heterogeneous oxidation of organic aerosol in the atmosphere is complex due in large part to both the rich array of organic molecules present in ambient aerosol and the numerous free radical transformation pathways initiated by gas phase oxidants (e.g., hydroxyl (OH), nitrate (NO_3), and chlorine (Cl) radicals).[1,2] Gas and condensed phase reaction mechanisms are typically used to interpret the formation of particle phase products, yet it remains unclear how well these reaction mechanisms explain heterogeneous aerosol oxidation, which is controlled to a large extent by particle phase properties such as radical chain propagation reactions, thermodynamic phase, and interfacial molecular orientation.[3−6]

Received: August 19, 2014
Revised: November 11, 2014
Published: November 11, 2014

   dx.doi.org/10.1021/jp508378z | J. Phys. Chem. A 2014, 118, 11555−11571

To better understand fundamental OH-particle reactions, several studies have investigated the products formed in the OH reaction with saturated organic aerosol.[4,5,7−15] These studies found that oxidation proceeds via the abstraction of a hydrogen (H) atom by an OH radical to form an alkyl radical. In the presence of O_2, the alkyl radical rapidly forms a peroxy radical, which reacts through a series of functionalization and fragmentation pathways to form higher and lower molecular weight oxygenated products. Functionalization reactions produce less volatile higher molecular weight products via the addition of oxygenated functional groups (e.g., carbonyl and hydroxyl groups) to the carbon backbone. Conversely, fragmentation reactions produce lower molecular weight oxygenated products via C−C bond scission along the carbon backbone.

The distribution of products formed from heterogeneous oxidation depends strongly on molecular structure. Ruehl et al.[4] analyzed the products formed by the reaction of OH with squalane (a liquid branched C_{30} alkane) and octacosane (a solid normal C_{28} alkane) aerosols and observed that the first generation squalane and octacosane functionalization products consist primarily of carbonyls and alcohols. Additionally, they observed that the squalane reaction yielded significantly more fragmentation products than octacosane. The carbon number distribution of the squalane fragmentation products is consistent with C−C bond scission reactions involving tertiary carbons, so the smaller amount of octacosane fragmentation products is attributed to the lack of tertiary carbons in octacosane. Zhang et al.[13] showed that the heterogeneous reaction of OH with cholestane (a $C_{27}H_{48}$ solid cyclic alkane with a branched aliphatic side chain) yielded few ring-opening oxidation products. This is in contrast to gas phase reaction mechanisms,[16−21] which predict that ring-opening products would be formed in large abundance due to the presence of highly reactive tertiary and secondary carbons in the aliphatic ring. These studies clearly indicate that the influence of molecular structure on heterogeneous reaction mechanisms is still not well understood and should be an area of focus for future studies.

Unlike H atom abstraction by OH of aerosol composed of saturated organic molecules, the heterogeneous OH-initiated oxidation of unsaturated organic species mainly proceeds primarily via OH addition to a C═C double bond to form a hydroxyalkyl radical.[22−25] Previous kinetic studies of the oxidation of unsaturated C_{18} fatty acids (oleic acid, linoleic acid and linolenic acid)[24] and squalene[25] aerosols reported that the hydroxyalkyl radical reacts though a sequence of intermediates to form functionalization and fragmentation products, a result broadly consistent with previous gas[16,17,21] and monolayer[22,23] studies. In addition, the effective uptake coefficients, defined as the number of particle phase molecules reacted per OH-particle collision, are found to be larger than one for these reactions, providing clear evidence for particle-phase secondary chain chemistry. These secondary chain reactions may in turn alter the distribution of functionalization and fragmentation particle phase products. Furthermore, the formation of hydroxyperoxy radicals (from the reaction of hydroxyalkyl radicals with O_2), and their subsequent reaction pathways to form stable products, provides a means of understanding how reaction mechanisms might be altered by the presence of adjacent oxygenated functional groups, which is a common molecular feature in highly oxygenated organic aerosol.[10,26]

This work aims to provide new molecular and mechanistic insights into the reaction pathways in the heterogeneous OH-initiated oxidation of unsaturated organic aerosol through detailed product analysis. Aerosols of squalene ($C_{30}H_{50}$, a liquid branched alkene with six C═C double bonds) and linolenic acid ($C_{18}H_{30}O_2$, a liquid linear carboxylic acid with three C═C double bonds) are photo-oxidized in a flow reactor and analyzed using two-dimensional gas chromatography coupled to electron impact ionization and vacuum ultraviolet photo-ionization mass spectrometry. This technique separates and quantifies the products by their volatility, polarity and mass spectra. Figure 1 shows the molecular structures of squalene and linolenic acid. The carbon atoms in the carbon backbones of both molecules are labeled and will be referred to accordingly in this paper.

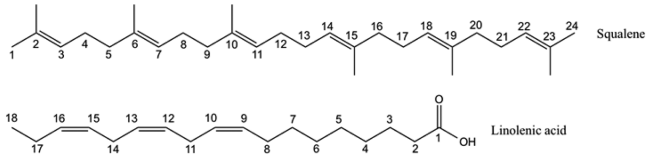

Figure 1. Molecular structures of squalene and linolenic acid. The carbon atoms in the carbon backbones of both molecules are labeled and will be referred to accordingly in this paper.

and linolenic acid. The carbon atoms in the carbon backbones of both molecules are labeled and referred to accordingly throughout this paper. By measuring both reactions at high and low $[O_2]$ (~1% vs 10% $[O_2]$), information can be obtained about the roles of hydroxyalkyl and hydroxyperoxy radical intermediates in product formation. This work builds on our previous investigations, which focused broadly on the heterogeneous chemical kinetics of the linolenic acid[24] and squalene[25] reactions. Here we focus on the molecular and positional isomeric distributions of the particle phase functionalization and fragmentation products and how their relative populations depend upon $[O_2]$. As such the identities and relative abundances of squalene and linolenic acid oxidation products provide a more comprehensive understanding of how molecular structure (branched vs linear) influences product distributions in the heterogeneous oxidation of unsaturated organic aerosol. Even though gas phase products are not directly measured in this study, the importance of fragmentation reactions can still be inferred through detailed analysis of the particle phase fragmentation products.

2. EXPERIMENT

2.1. Flow Tube Reactor Experiments. The experimental setup used in this study has been described in detail previously[24,25] and will be reviewed briefly here. An atmospheric pressure flow reactor (1.4 m long, 5.8 cm i.d., quartz tube) is used to investigate the heterogeneous oxidation of squalene and linolenic acid aerosol. OH radicals are generated in the flow reactor via the photolysis of H_2O_2 gas using four continuous output 130 cm long Hg lamps (λ = 254 nm) that are placed outside and along the length of the flow reactor. Aerosol particles are generated by homogeneous nucleation in a N_2 stream flowing through a pyrex tube (heated in a furnace at 135 and 112 °C for squalene and linolenic acid, respectively) containing either liquid squalene or linolenic acid. The aerosol stream is passed through an annular activated charcoal denuder to remove any residual gas phase organics that may have been formed in the furnace. A N_2/H_2O_2 gas mixture is introduced into the reactor by passing 0.15 L/min of N_2 through a heated bubbler (50 °C) that is packed with

dx.doi.org/10.1021/jp508378z | J. Phys. Chem. A 2014, 118, 11555−11571

a 50:50 mixture of sand and urea-hydrogen peroxide. Additional flows of humidified N_2, O_2 and tracer gas hexane (~150 ppb hexane in the flow reactor) are added to give a total flow rate of 1 L/min entering the flow reactor. The relative humidity in the flow reactor is fixed at 30%. The $[H_2O_2]$ in the flow reactor prior to reaction is ~1 ppm. The $[O_2]$ in the flow reactor are reported here as flow ratios (e.g., 10% $[O_2]$ is obtained when 0.1 L/min of the total 1 L/min flow is O_2).

The OH exposure in the flow reactor is changed by adjusting the photon flux of the Hg lamps while keeping the total flow rate constant. The OH exposure in the flow reactor is determined from the decay of the tracer gas hexane, which is measured using a gas chromatograph equipped with a flame ionization detector (SRI Instruments), as described previously by Smith et al.[12] On the basis of the illuminated volume of the reactor and the total flow rate going into the reactor (1 L/min), the reaction time is ~220 s. OH concentrations in the flow reactor range from 7×10^7 to 9×10^8 mol cm^{-3}. Particle size distributions exiting the flow reactor are measured by a scanning mobility particle sizer (SMPS, TSI model 3772). The squalene and linolenic acid particle size distributions are log-normal, with total mass concentrations of ~8000 μg/m^3, and mean surface weighted diameters of ~170 and 190 nm, respectively. The mass concentrations of unreacted squalene and linolenic acid (~8000 μg/m^3) are obtained from the SMPS data using the densities of squalene (0.858 g/cm^3) and linolenic acid (0.914 g/cm^3), respectively. At each OH exposure, aerosol samples are collected for ~30 min at 0.6 L/min onto quartz filters (4.7 cm diameter Tissuquartz, Pall Life Science, prebaked at 600 °C). The aerosol stream is passed through a charcoal denuder (8 in. 480-channel MAST Carbon) before the filters to prevent gas phase compounds from adsorbing onto the filters. Particle phase organic compounds with less than ~10 carbon atoms are expected to be removed from the particle via evaporation by the charcoal denuder.

2.2. Two-Dimensional Gas Chromatography with High-Resolution Time-of-Flight Mass Spectrometry. The gas chromatograph used to analyze the filters has been described in detail previously[4,13,27] and will be discussed briefly here. Prior to analysis the filters are stored at −20 °C. The filters are analyzed using two-dimensional gas chromatography and detected by high-resolution time-of-flight mass spectrometry utilizing either electron impact (EI) ionization or vacuum ultraviolet (VUV) photoionization (GC × GC-HRTOF-EI/VUVMS). The filters (sampled area = 0.41 cm^2) are thermally desorbed at 320 °C in helium using a thermal desorption system and autosampler (TDS3 and TDSA2, Gerstel) and introduced into a two-dimensional gas chromatograph (GC × GC, Agilent 7890). The helium stream is saturated with the *N*-methyl-*N*-trimethylsilyl trifluoroacetamide (MSTFA) derivatization reagent to convert hydroxyl groups into trimethylsilyl ethers that are amenable to GC analysis.

Analytes are first separated by volatility using a 60 m × 0.25 mm × 0.25 μm nonpolar capillary column (Rxi-5Sil MS, Restek, 85 min retention time), then by polarity using a 1 m × 0.25 mm × 0.25 μm medium polarity column (Rtx-200MS, Restek, 2.3 s retention time). The first column is connected to the second column using a dual loop modulator (1.5 m × 0.25 mm Rxi guard column, Zoex Corp, 2.4 s modulation time). Internal standards of deuterated *n*-alkanes are used to correct for GC column transfer efficiency and chromatogram reproducibility. Mass spectra are obtained using a high-resolution ($\Delta m/m \sim 4000$) time-of-flight mass spectrometer (ToFWerk) using either EI ionization (70 eV) or VUV photoionization (10.5 eV). The VUV radiation is produced by the Chemical Dynamics Beamline at the Advanced Light Source.

EI-MS and external standards are used with MSTFA derivatization to calculate the response factors for GC × GC chromatographic analysis and quantify oxidation products. Since analytical standards are not commercially available for the quantification of squalene and linolenic acid oxidation products, external standards with retention times similar to these products are used instead. This adds to the uncertainty of the product quantification since the squalene and linolenic acid oxidation products may have different response factors from the external standards. This is especially true for linolenic acid oxidation products, which have three or more oxygenated functional groups, since the external standards used in this study have only one or two oxygenated functional groups and may not be suitable for accurate quantification of highly oxygenated compounds due to differing response factors. In addition, the response factors tend to decrease with decreasing volatility and increasing polarity for the GC system used in this study.[4] Highly oxygenated compounds (with three or more oxygenated functional groups) may also have lower GC column transfer efficiencies.[13] In this study, external standards of 12-hydroxyoctadecanoic acid, palmitic acid, margaric acid, stearic acid and behenic acid are used to correct for the volatility response of linolenic acid products with alcohol functional groups. Standards of triacontane, 1-hexadecanol, 1-octadecanol and 1-eicosanol are used to correct for the volatility response of squalene oxidation products with alcohol functional groups. These standards are chosen since they have similar polarities as these oxidation products (with alcohol functional groups) when MSTFA is used as the derivatization reagent. 2-Pentadecanone and 2-octadecanone standards are used correct for the polarity response of squalene and linolenic acid oxidation products with carbonyl functional groups.

VUV-MS is used to identify specific compounds and structural isomers. The VUV mass spectrum generally features a more prominent molecular ion peak and significantly fewer fragment ions compared to EI. Although the molecular formulas of the compounds are determined from high-resolution VUV mass spectra, for simplicity, only integer m/z values are presented in this paper. Shown as an example in Figure S1 (Supporting Information) are VUV mass spectra obtained for derivatized linolenic acid (Figure S1a) and its diol products (Figure S1b−d). Using MSTFA as the derivatization reagent results in the acidic H atoms in alcohol and carboxylic acid functional groups to be substituted by a trimethylsilyl ($Si(CH_3)_3$, labeled as "TMS") group. For simplicity, the TMS-derivatized hydroxyl (OH) groups in alcohol and carboxylic acid functional groups are labeled as "OTMS" in this paper. In Figure S1 (Supporting Information), the molecular ions of linolenic acid ($C_{17}H_{29}COOH$, m/z 278) and its diol product isomers ($C_{17}H_{29}CO(OH)_3$, m/z 312) appear as $C_{17}H_{29}CO$-(OTMS) (m/z 350) and $C_{17}H_{29}CO(OTMS)_3$ (m/z 528), respectively.

3. RESULTS AND DISCUSSION

The product analysis of the squalene and linolenic acid reactions are discussed in sections 3.1 and 3.2, respectively. Section 3.1.1 provides an overview of the squalene two-dimensional GC (GC × GC) chromatogram. In this section the oxidation products are presented in broad groupings by

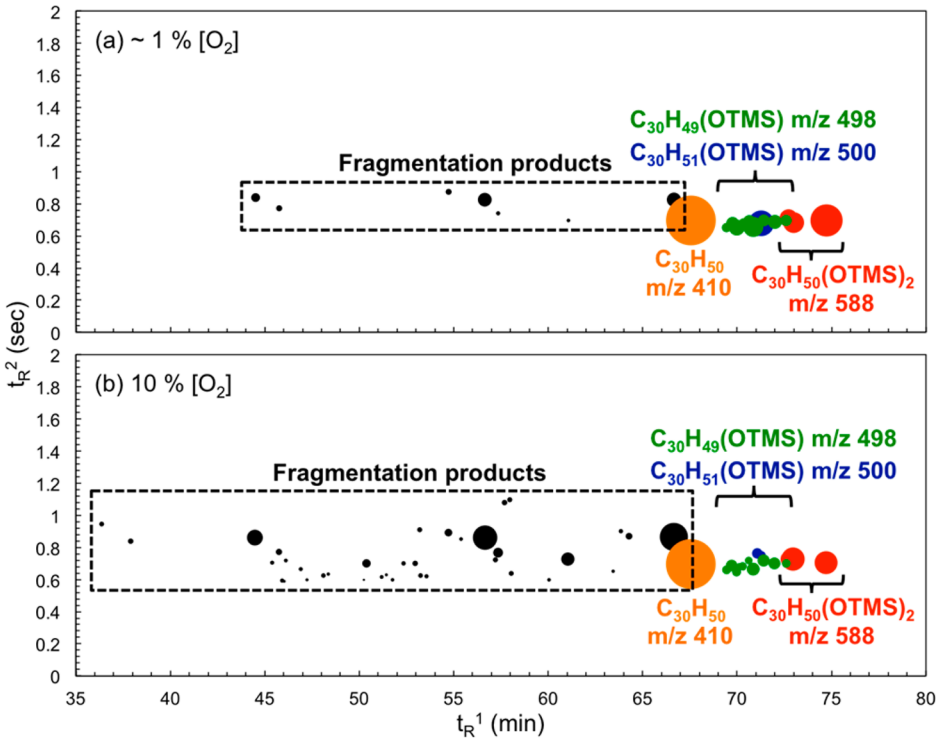

Figure 2. Relative abundance of squalene and its oxidation products shown in GC × GC space at OH exposure =1.62 × 10^{11} molecules cm^{-3} s at (a) ~ 1% and (b) 10% [O_2]. The *x*-axis is the first dimension (t_R^1) and the *y*-axis is the second dimension (t_R^2) retention time. In panels a and b, each circle represents a single compound and its relative abundance is represented by the size of the circle. Squalene $C_{30}H_{50}$ is the orange circle located at t_R^1 ~ 67.5 min and t_R^2 ~ 0.7 s. The oxidation products are separated into four groups by their chemical formulas and delineated with different colors: all fragmentation products (black); derivatized $C_{30}H_{49}$(OTMS) alcohols (green); derivatized $C_{30}H_{51}$(OTMS) alcohols (blue); derivatized $C_{30}H_{50}(OTMS)_2$ diols (red).

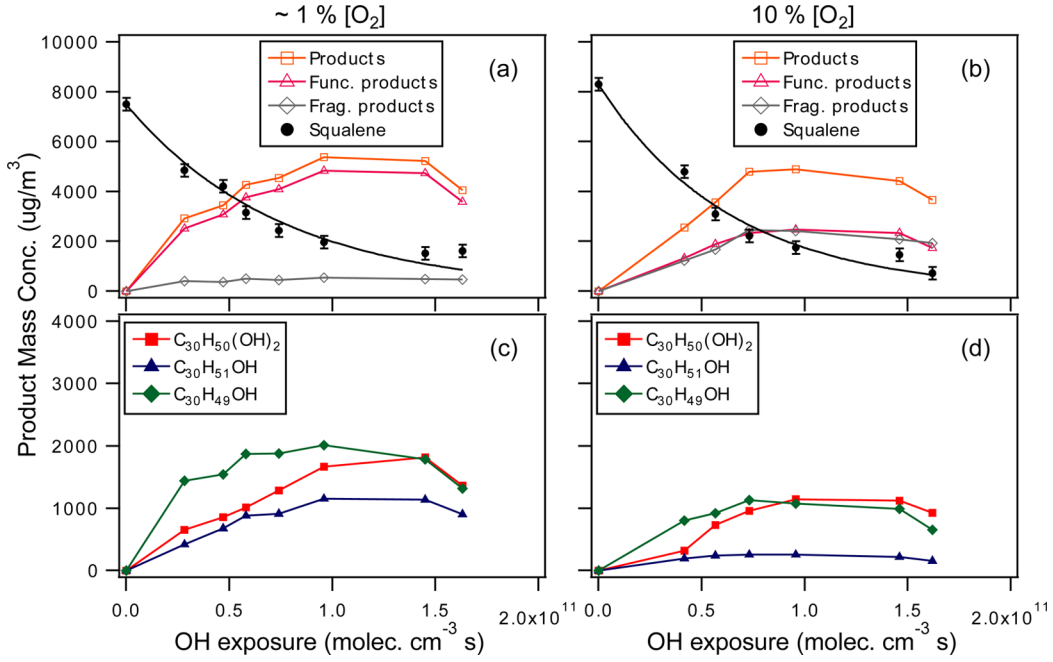

Figure 3. Total mass concentrations of squalene, oxidation products, functionalization products and fragmentation products as a function of OH exposure at (a) ~ 1% [O_2], and (b) 10% [O_2]. Error bars for the squalene mass concentrations originate from the filter sampling process. The squalene decays in parts a and b are fit to an exponential function. Total mass concentrations of $C_{30}H_{49}OH$ alcohol, $C_{30}H_{51}OH$ alcohol and $C_{30}H_{50}(OH)_2$ diol products as a function of OH exposure at (c) ~ 1% [O_2], and (d) 10% [O_2].

molecular formula (i.e., functionalization and fragmentation) to show in a general way how the aerosol composition evolves as a function of OH exposure. This overview is followed by detailed isomeric analysis of individual products: $C_{30}H_{51}OH$ and $C_{30}H_{49}OH$ alcohols (3.1.2) and $C_{30}H_{50}(OH)_2$ diols (3.1.3). In section 3.1.4, the carbon number distribution of the squalene

dx.doi.org/10.1021/jp508378z | J. Phys. Chem. A 2014, 118, 11555−11571

fragmentation products is presented. Section 3.2 on the linolenic acid reaction is similarly subdivided into an overview of the linolenic acid GCXGC chromatogram (3.2.1), isomeric product analysis of $C_{17}H_{30}CO(OH)_2$ and $C_{17}H_{28}CO(OH)_2$ alcohols (3.2.2), $C_{17}H_{28}CO_2(OH)_2$ hydroxycarbonyls and $C_{17}H_{29}CO(OH)_3$ diols (3.2.3), and fragmentation products (3.2.4).

3.1. Squalene Oxidation Product Analysis. *3.1.1. Squalene GC × GC Chromatogram.* Single ion chromatograms (extracted from the GC × GC run performed using VUV-MS) are used to identify product isomers via their molecular ions and resolve coeluting species. These product isomers are then quantified in EI-MS using their total GC volumes. Figure 2 shows the distribution and relative abundance of particle phase squalene oxidation products in GC × GC space (volatility t_R^1 vs polarity t_R^2) at an OH exposure of 1.6×10^{11} mol cm^{-3} s for ~1% and 10% [O_2] (Figure 2, parts a and b, respectively). Each circle signifies a single compound while its relative abundance is represented by the size of the circle.

Squalene $C_{30}H_{50}$ (m/z 410, shown in orange in Figure 2) elutes at first-dimensional retention time (t_R^1) ~ 67.6 min and second-dimensional retention time (t_R^2) ~ 0.7 s. Fragmentation products (shown in black in Figure 2) have carbon numbers less than 30 and elute at shorter t_R^1 relative to squalene, indicating that they are more volatile than squalene. The most prominent fragmentation products have carbon numbers 17, 22, and 27 (discussed in detail in section 3.1.4). Functionalization products with carbon number 30 and new oxygenated functional groups (formed in the reaction) elute at longer t_R^1 relative to squalene.

The functionalization products are grouped based on their molecular formulas. At both ~1% and 10% [O_2], two distinct groups of TMS-derivatized alcohol products are detected: $C_{30}H_{49}$(OTMS) (m/z 498, shown in green in Figure 2) and $C_{30}H_{51}$(OTMS) (m/z 500, shown in blue in Figure 2). Twelve $C_{30}H_{49}$(OTMS) alcohol isomers are resolved at t_R^2 ~ 0.7 s with t_R^1 from ~68 to 73 min. Three $C_{30}H_{51}$(OTMS) alcohol isomers are detected at t_R^2 ~ 0.7 s with t_R^1 from ~70 to 72 min. Three TMS-derivatized $C_{30}H_{50}$(OTMS)$_2$ diol isomers (m/z 588, shown in red in Figure 2) are also detected at t_R^2 ~ 0.7 s with t_R^1 from ~73 to 75 min. MSTFA derivatization decreases the polarity of the alcohol and diol products, causing them to have approximately the same t_R^2 as squalene.

The relative abundance of particle phase reaction products at ~1% and 10% [O_2] suggests that [O_2] controls the formation pathways of functionalization and fragmentation products. To obtain a more comprehensive understanding of how [O_2] influences the competition between functionalization and fragmentation pathways, the mass concentrations of detected squalene particle phase oxidation products are quantified using external standards. Parts a and b of Figure 3 show the mass concentrations of squalene and its detected oxidation products, which are subdivided into total functionalization and fragmentation products, as a function of OH exposure at ~1% and 10% [O_2], respectively. Error bars for the oxidation product mass concentrations are not shown since there is some uncertainty on how the detection efficiencies of the external standards differ from that of the products.

Figure 3a shows that at ~1% [O_2] the total mass concentration of detected oxidation products increases and reaches a maximum value of ~5370 μg/m^3 at an OH exposure of ~9.6×10^{10} molecules cm^{-3} s, before decreasing upon further oxidation. Approximately 89% of the observed oxidation products are functionalization products, and approximately 11% are fragmentation products. This indicates that the addition of oxygenated functional groups to the carbon backbone (i.e., functionalization) dominates the heterogeneous reaction at ~1% [O_2].

Figure 3b shows that at 10% [O_2] the total mass concentration of detected oxidation products reaches a maximum value of ~4900 μg/m^3 at an OH exposure of ~9.6×10^{10} molecules cm^{-3} s, before decreasing upon further oxidation. Under these conditions, the total abundance of observed functionalization products is approximately equal to the fragmentation products, indicating that C−C bond cleavage (i.e., fragmentation) is important in the presence of 10% [O_2].

The total mass concentration of detected oxidation products is compared to the reactive loss of squalene. At ~ 1% [O_2] (Figure 3a), ~ 90% of the original squalene mass concentration can be accounted for (by particle phase products and unreacted squalene) over the course of the reaction. The remaining mass can be attributed to gas phase fragmentation products (which are not collected on filters). At 10% [O_2] (Figure 3b), only ~80% of the original squalene mass concentration can be accounted for during oxidation. This is likely due to particle volatilization being an important reaction channel at high [O_2], as demonstrated by the detection of higher mass concentrations of fragmentation products at 10% [O_2]. This is also consistent with aerosol mass measurements presented previously by Nah et al.,[25] which showed that significant particle volatilization occurs at high [O_2] in the squalene reaction (~5% particle mass loss at ~0% [O_2] vs ~20% particle mass loss at 10% [O_2]).

The squalene mass concentration vs OH exposure (Figure 3, parts a and b) can be fit by an exponential function. Similar to the previous kinetics study of the squalene reaction,[25] these exponential decays indicate that the decay rate is directly proportional to the concentration of particle phase squalene and the reaction is not limited by the diffusion of squalene molecules to the particle surface. As described previously by Nah et al.,[25] the squalene decay rate constants can be used to calculate an effective uptake coefficient (γ_{OH}^{Sqe}). Using the methodology detailed in Nah et al., γ_{OH}^{Sqe} measured at ~1% and 10% [O_2] are 2.92 ± 0.18 and 3.65 ± 0.22, respectively. This indicates that more than one particle phase squalene molecule is lost for every OH-particle collision and is clear evidence for secondary chain chemistry. Because of unknown amounts of secondary chemistry, the γ_{OH}^{Sqe} values are not corrected for gas phase diffusion.

The measured γ_{OH}^{Sqe} values are larger than those previously reported by Nah et al.[25] (1.55 ± 0.05 and 2.59 ± 0.12 for 1.4 ppm [H_2O_2] at ~0% and 10% [O_2], respectively). These differences most likely arise from differences in the radical chain propagation length, whose magnitude is sensitive to reaction time and oxidant concentration. For example, previously it has been shown that γ_{OH}^{Sqe} is highly dependent on O_2, H_2O_2 and OH concentrations in the reactor.[25] In this study, the reaction time is longer and the average [OH] in the flow reactor is smaller than those used in Nah et al.[25] Che et al.[14] observed larger effective uptake coefficients in the OH + squalane reaction when longer reaction times and lower average [OH] are used, and they attributed this to secondary reactions. Here it is possible that the differences in the experimental conditions led to differences in the radical chain propagation length, and consequently differences in the γ_{OH}^{Sqe} values. Nonetheless the increase in γ_{OH}^{Sqe} when [O_2] increases from ~1% to 10% in this study is broadly consistent with the previous study of the

squalene reaction[25] and indicates that O_2 promotes chain propagation.

The observed functionalization products are composed of TMS-derivatized $C_{30}H_{49}(OTMS)$, $C_{30}H_{51}(OTMS)$ and $C_{30}H_{50}(OTMS)_2$ product isomers. The underivatized molecular formulas of these products (obtained by substituting the "TMS" group with a H atom) are $C_{30}H_{49}OH$, $C_{30}H_{51}OH$ and $C_{30}H_{50}(OH)_2$, respectively. Previous kinetic studies[25] indicate that these are first generation functionalization products. Parts c and d of Figure 3 show the evolution of $C_{30}H_{49}OH$, $C_{30}H_{51}OH$, and $C_{30}H_{50}(OH)_2$ as a function of OH exposure at ~1% and 10% $[O_2]$, respectively. At ~ 1% $[O_2]$, $C_{30}H_{49}OH$, $C_{30}H_{51}OH$ and $C_{30}H_{50}(OH)_2$ make up approximately 46%, 22% and 32% of the total mass concentration of detected functionalization products, respectively (Figure 3c). At 10% $[O_2]$, $C_{30}H_{49}OH$, $C_{30}H_{51}OH$ and $C_{30}H_{50}(OH)_2$ make up approximately 47%, 11%, and 42% of the total mass concentration of detected functionalization products, respectively (Figure 3d). Carbonyls and TMS-derivatized hydroxycarbonyls are not detected at either ~1% or 10% $[O_2]$, indicating that they are minor reaction products.

The formation of first generation $C_{30}H_{49}OH$, $C_{30}H_{51}OH$, and $C_{30}H_{50}(OH)_2$ functionalization products, together with the absence of hydroxycarbonyl products in the GC × GC chromatogram and the increased abundance of fragmentation products at 10% $[O_2]$ (relative to at ~1% $[O_2]$) oxidation can be explained by the reaction mechanism proposed previously by Nah et al.[25] In that work, it is shown that the OH + squalene reaction is initiated predominantly by OH addition to the less substituted carbon of the C=C double bond to form tertiary hydroxyalkyl radicals. Figure 4 shows the reaction mechanism

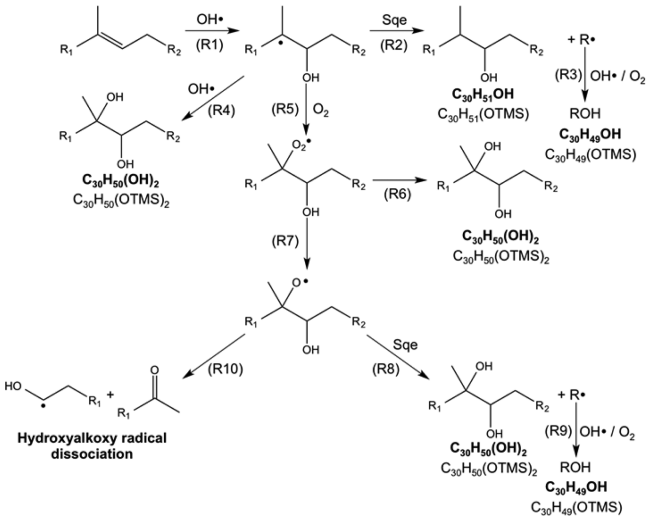

Figure 4. Reaction mechanism for the OH-initiated oxidation of squalene (Sqe) aerosol. R• represents the generic alkyl radical formed by the abstraction of a H atom from a squalene molecule. The underivatized (bold text) and derivatized (regular text) molecular formulas of the detected first generation functionalization products are also shown.

for the OH-initiated oxidation of squalene aerosol. For clarity, the derivatized and underivatized molecular formulas of the products are also shown. This reaction scheme is used to understand the distribution of isomeric products described in sections 3.1.2−3.1.4.

Although the hydroxyalkyl/alkyl radical + hydroxyperoxy/peroxy radical (R + RO_2), hydroxyalkyl/alkyl radical + hydroperoxyl radical (R + HO_2) and hydroxyperoxy/peroxy radical + hydroperoxyl radical (RO_2 + HO_2) reactions (which form organic peroxides ROOR and ROOH) have been observed in gas phase reactions,[16,17,21] we see no evidence of ROOR and ROOH products in this study despite the estimated average $[HO_2]$ being approximately equal to the average [OH] in the flow reactor (estimated using a kinetic model). ROOR and ROOH products are also not detected in our previous study of the squalene reaction.[25] Therefore, these chain termination reactions appear to be minor channels, within our ability to detect these products, in the squalene reaction, and are not included in the reaction mechanism presented in Figure 4. It is possible that the measurement techniques used in this study and our previous study of the squalene reaction[25] may not be sensitive to ROOR and ROOH products, however similar observations that the R + RO_2, R + HO_2, and RO_2 + HO_2 reactions are potentially minor channels in heterogeneous reactions have been made in previous heterogeneous aerosol oxidation studies by Smith et al.,[12] McNeill et al.,[11] and Ruehl et al.[4] The reactions of hydroxyalkoxy and alkoxy radicals with HO_2 radicals to form hydroxycarbonyls and carbonyls, respectively, are also important pathways in gas phase reactions.[16,17,21] However, carbonyls and hydroxycarbonyls are not detected in the squalene GC × GC chromatograms. This suggests that they are likely minor channels in the squalene reaction, and are therefore not included in the reaction mechanism shown in Figure 4.

It is important to note that high [OH] and short reaction times (with respect to ambient conditions) are used in this product formation study. These experimental conditions may cause the measured branching ratios among the various reaction pathways to differ from that observed in the atmosphere. For example, the importance of hydroxyperoxy radical self- and cross-reactions may be larger in this study than in ambient conditions due to the higher radical concentrations used here. Nonetheless, since the experimental conditions employed in this study for squalene and linolenic acid oxidation are similar, we can directly compare the identities and relative abundances of squalene and linolenic acid oxidation products to gain an understanding of how molecular structure (branched vs linear) influences product distributions in the heterogeneous oxidation of unsaturated organic aerosol.

3.1.2. $C_{30}H_{51}OH$ and $C_{30}H_{49}OH$ Alcohol Product Isomers. Three TMS-derivatized $C_{30}H_{51}(OTMS)$ alcohol isomers are detected at ~1% and 10% $[O_2]$. The underivatized molecular formula of these alcohol isomers $C_{30}H_{51}OH$ indicates that one O atom and two H atoms are added to the squalene molecule. On the basis of the reaction mechanism shown in Figure 4, these $C_{30}H_{51}OH$ alcohol products are formed via R2 where a H atom is abstracted from a neighboring squalene molecule by the hydroxyalkyl radical.

At ~ 1% $[O_2]$, the total mass concentration of $C_{30}H_{51}OH$ alcohol isomers increases to a maximum of ~1150 $\mu g/m^3$ (OH exposure ~9.6×10^{10} molecules cm^{-3} s, Figure 3c). At 10% $[O_2]$, the total mass concentration of $C_{30}H_{51}OH$ alcohol isomers reaches a maximum of ~260 $\mu g/m^3$ (OH exposure ~7.3×10^{10} molecules cm^{-3} s, Figure 3d). Thus, the total abundance of these alcohol isomers is approximately four times larger at ~1% $[O_2]$ compared to 10% $[O_2]$, indicating that increasing O_2 suppresses their formation pathways. This is consistent with the reaction mechanism (Figure 4), where the

dx.doi.org/10.1021/jp508378z | J. Phys. Chem. A 2014, 118, 11555−11571

formation of hydroxyperoxy radicals (R5) becomes the dominant reaction pathway for hydroxyalkyl radicals at high $[O_2]$, effectively slowing down R2, the chain propagation reaction that produces $C_{30}H_{51}OH$ alcohol products.

Parts a–c of Figure 5 show the VUV mass spectra of the three detected TMS-derivatized $C_{30}H_{51}(OTMS)$ (m/z 500)

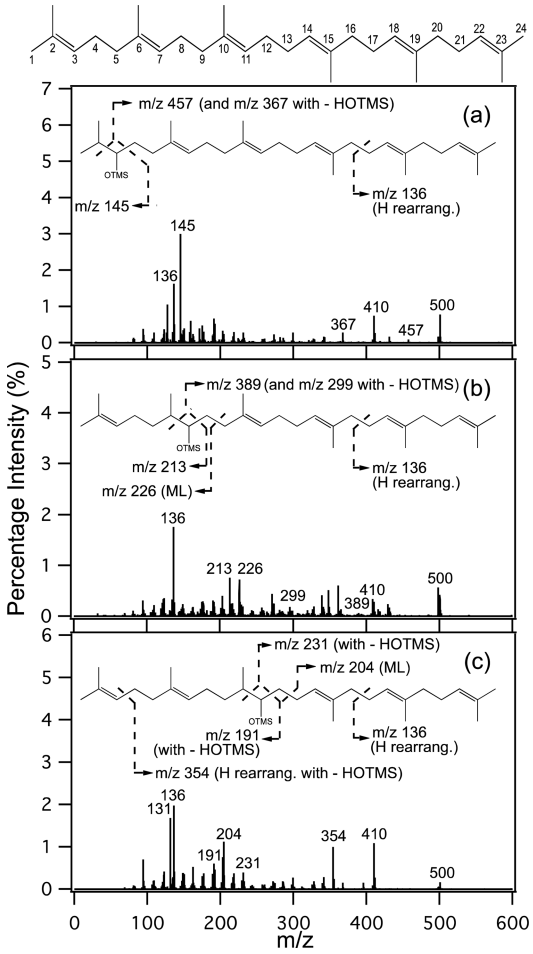

Figure 5. (a–c) VUV mass spectra of the TMS-derivatized $C_{30}H_{51}(OTMS)$ alcohol product isomers (m/z 500). Figure insets in panels a–c show the ion fragmentation patterns that explain the characteristic ion peaks observed in the mass spectra. The McLafferty rearrangement and H rearrangement are labeled as "ML" and "H rearrang." respectively. In panels a–c, the m/z 410 fragment ion is formed from the loss of HOTMS. The ion peak m/z 131 in panel c is a C_3H_6OTMS fragment. Also shown are the labeled carbon atoms in the squalene carbon backbone.

alcohol isomers. Also shown are the ion fragmentation patterns that explain the characteristic ion peaks observed in the VUV mass spectra. The observed fragment ions in the mass spectra are produced by α-cleavage, β-cleavage, McLafferty rearrangement, and H rearrangement. The m/z 410 ion is a prominent fragment ion in the three VUV mass spectra, and it corresponds to the loss of $(CH_3)_3SiOH$ (labeled "HOTMS"). The loss of HOTMS is similar to the dehydration of alcohols. Similar fragment ions in the VUV mass spectra of TMS-derivatized alcohols have also been observed by Zhang et al.[13] in their study of cholestane aerosol oxidation.

By identifying distinct fragment ions in the VUV mass spectra of these three TMS-derivatized $C_{30}H_{51}(OTMS)$ alcohol isomers, the location of the OTMS group (and consequently the hydroxyl group) along the squalene carbon backbone can be ascertained. For example, Figure 5a shows the VUV mass spectrum of a TMS-derivatized $C_{30}H_{51}(OTMS)$ alcohol isomer with an OTMS group on C3 of the squalene carbon backbone. The α-cleavage process is the dominant ion fragmentation pathway, producing m/z 145 ($C_4H_8(OTMS)^+$) and 457 ($C_{27}H_{44}(OTMS)^+$) fragment ions. Using this approach, the VUV mass spectra shown in Figure 5, parts b and c, are determined to be $C_{30}H_{51}(OTMS)$ alcohol isomers with an OTMS group on C7 and C11 of the squalene carbon backbone, respectively. Together these mass spectra indicate that these three alcohol isomers all originate from OH addition to the less substituted carbon of the C=C double bond.

$C_{30}H_{51}(OTMS)$ alcohol isomers with the OTMS group on C11 of the squalene carbon backbone make up the majority (~50%) of the structural isomers. This suggests that $C_{30}H_{51}OH$ alcohol isomers with the hydroxyl group on C11 of the squalene carbon backbone are formed preferentially (compared to the other two isomers) during the reaction. It is currently unclear why this is the case and should be an area of focus for further investigation.

$C_{30}H_{51}(OTMS)$ alcohol isomers with OTMS groups located on C2, C6 and C10 of the squalene carbon backbone are not detected, indicating that $C_{30}H_{51}OH$ isomers formed via OH addition to the more substituted carbon of the C=C double bond are minor reaction products. These results suggest more generally that OH addition occurs at the less substituted carbon of the C=C double bond (to form tertiary hydroxyalkyl radicals), while OH addition to the more substituted carbon of the C=C double bond (to form secondary hydroxyalkyl radicals) is a minor channel. OH addition to the less substituted carbon of the C=C double bond is also the dominant channel in the oxidation of gas phase unsaturated organics by OH radicals.[19]

The higher propensity for OH addition to the less substituted carbon of the C=C double bond is also consistent with the absence of TMS-derivatized $C_{30}H_{49}O(OTMS)$ hydroxycarbonyl products from the GC × GC chromatogram and the large abundance of fragmentation products at 10% $[O_2]$. On the basis of the reaction mechanism shown in Figure 4, the preference for OH addition to the less substituted carbon of the C=C double bond leads to high yields of tertiary hydroxyperoxy radicals (relative to secondary hydroxyperoxy radicals) at high $[O_2]$ (R5). The formation of hydroxycarbonyl products (via the Russell and Bennett–Summers mechanisms[28−32]) is suppressed in the tertiary hydroxyperoxy radical self-reaction due to the lack of H atoms adjacent to the peroxy radical site. Instead tertiary hydroxyalkoxy radicals are likely the dominant products from tertiary hydroxyperoxy radical self-reaction (R7). These tertiary hydroxyalkoxy radicals can dissociate to form fragmentation products (R10), which may explain the high yields of fragmentation products at 10% $[O_2]$ (relative to ~1% $[O_2]$).

In addition to self-reaction, tertiary hydroxperoxy radicals can also react with secondary hydroxyperoxy radicals and peroxy radicals (formed from the reaction of O_2 with alkyl radicals that are formed in reactions R2 and R8) to form diols (R6) and tertiary hydroxyalkoxy radicals (R7). As discussed above, our results suggest that secondary hydroxyalkyl and hence secondary hydroxyperoxy radicals are formed in low abundance relative to tertiary hydroxyalkyl and tertiary hydroxyperoxy radicals. Therefore, the reaction between tertiary and secondary hydroxyperoxy radicals is expected to be minor channel, while

dx.doi.org/10.1021/jp508378z | J. Phys. Chem. A 2014, 118, 11555−11571

reactions between tertiary hydroxyperoxy radicals and peroxy radicals are expected to play more important roles in product formation. This is another reason for the absence of TMS-derivatized $C_{30}H_{49}O$(OTMS) hydroxycarbonyl products from the GC × GC chromatogram.

The role that tertiary hydroxyalkoxy radical intermediates plays in radical chain chemistry at high $[O_2]$ is demonstrated by the measured γ_{OH}^{Sqe}, which increases from 2.92 ± 0.18 at ∼1% $[O_2]$ to 3.65 ± 0.22 at 10% $[O_2]$. On the basis of the reaction mechanism shown in Figure 4, pathways R2 and R8 are chain propagation reactions that accelerate the reactive depletion of squalene molecules at high $[O_2]$. At low $[O_2]$, pathway R8 is suppressed since hydroxyperoxy radicals (and consequently hydroxyalkoxy radicals) are formed in low abundance. Therefore, the radical chain chemistry in the particle is slowed with decreasing $[O_2]$, causing γ_{OH}^{Sqe} to decrease when $[O_2]$ is decreased.

Twelve TMS-derivatized $C_{30}H_{49}$(OTMS) alcohol isomers are detected at ∼1% and 10% $[O_2]$. The underivatized molecular formula of these alcohol isomers $C_{30}H_{49}OH$ corresponds to the addition of one O atom to the squalene molecule. Figure 3, parts c and d show that the total mass concentration of $C_{30}H_{49}OH$ alcohol isomers reaches a maximum of ∼2010 $\mu g/m^3$ and ∼1130 $\mu g/m^3$ at an OH exposure of ∼9.6×10^{10} molecules cm^{-3} s at ∼1% and 10% $[O_2]$, respectively. On the basis of the reaction mechanism shown in Figure 4, these $C_{30}H_{49}OH$ alcohol product isomers are formed by the reaction of alkyl (R) radicals (formed by H atom abstraction reactions R2 and R8) with O_2 and OH radicals (R3 and R9). The R radicals react with O_2 to form peroxy radicals, which undergo self- and cross-reactions to form $C_{30}H_{49}OH$ alcohol products.[28−32] It is possible that the R radicals are also formed by H atom abstraction reactions by OH radicals (for brevity this pathway is not explicitly shown in Figure 4), even though studies by Atkinson et al.[33,34] suggest that this is a minor reaction pathway. It remains unclear how well these studies on small gas phase alkenes ($\leq C_5$) extrapolate to the heterogeneous oxidation of large alkenes (i.e., squalene).

Squalene has 44 H atoms in $C(sp^3)$−H bonds available for abstraction. Abstraction of H atoms attached to the C=C double bonds are expected to be energetically unfavorable.[35,36] The 44 H atoms from the $C(sp^3)$−H bonds in squalene are allylic as they are attached to C atoms adjacent to C=C double bonds. Equation 1 illustrates resonance stabilization of allylic R radicals formed from H atom abstraction.

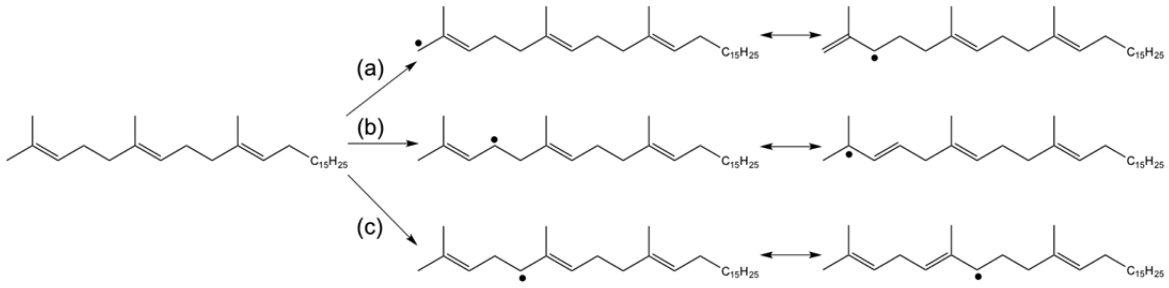

(1)

As a result of resonance stabilization, 16 allylic R radicals could be formed from H atom abstraction reactions (shown in Figure S2 in the Supporting Information). To qualitatively characterize the probability at which each resonance structure forms, quantum chemical calculations are performed using the Gaussian 09[37] program (shown and described in Figure S3 in the Supporting Information). A smaller C_7H_{14} squalene analogue with three allylic positions is used for these calculations, as high-level calculations of the larger molecule are unfeasible. The quantum chemical calculations show that the unpaired electron resulting from H atom abstraction is delocalized across the adjacent double bond (i.e., the electron density is evenly distributed) resulting in two regions of significant electron density as expected of an allylic R radical. This suggests that the resonance-stabilized allylic R radicals formed from intermolecular H atom abstraction reactions during squalene oxidation are delocalized. As a result one might expect to observe 16 $C_{30}H_{49}OH$ alcohol isomers formed from the reaction of allylic R radicals with O_2 and OH radicals. However, only 12 TMS-derivatized $C_{30}H_{49}$(OTMS) alcohol isomers are detected at ∼1% and 10% $[O_2]$.

One possible explanation for the detection of only 12 (instead of 16) TMS-derivatized $C_{30}H_{49}$(OTMS) alcohol isomers is that some of these alcohol isomers may have similar volatilities, causing them to coelute. It is also possible that some of the allylic R radicals (i.e., tertiary vs secondary vs primary) are more reactive toward O_2 and OH radicals than others, resulting in only 12 $C_{30}H_{49}OH$ alcohols being formed. It is important to note that without the resonance stabilization of allylic R radicals, only a maximum of eight different TMS-derivatized $C_{30}H_{49}$(OTMS) alcohol isomers would be observed. Therefore, the detection of 12 TMS-derivatized $C_{30}H_{49}$(OTMS) alcohol isomers demonstrates that these allylic R radicals undergo resonance stabilization. Since the mass spectra of these 12 isomers contain similar fragment ions, we are not able to assign structural isomers.

Previous studies[28−32,38] have shown that R radicals react with O_2 to form peroxy radicals, which self- and cross-react to form alcohol ($C_{30}H_{49}OH$) or carbonyl ($C_{30}H_{48}O$) products. $C_{30}H_{48}O$ carbonyls are not detected in the GC × GC chromatograms, indicating that they are minor reaction products. Previous condensed phase studies[32,38−40] have similarly observed the formation of excess alcohol products (relative to carbonyl products) from peroxy radical self-reaction. These studies reported that a labile tetroxide intermediate is formed by peroxy radical self-reaction. The subsequent homolytic cleavage of this tetroxide intermediate into carbonyls, alcohols and alkoxy radicals (i.e., Russell and Bennett−Summers mechanisms[28−32,38−40]) depends on the structure of the initial peroxy radical, the temperature of the reaction and the viscosity of the solution. Thus, the alcohol:carbonyl product ratios are also observed to be influenced by the temperature of the reaction and the viscosity of the solution. Although previous condensed phase stud-

ies[32,38,39] have reported alcohol:carbonyl ratios of up to 2, our study suggest that this ratio is significantly higher for the squalene reaction. Since the formation of alcohols via peroxy radical chemistry requires the abstraction of H atoms by peroxy radicals, the high alcohol:carbonyl ratio in this study suggests that the peroxy radicals may be abstracting H atoms from other species other than peroxy radicals. While it is possible that, analogous to condensed phase studies, molecular structure, temperature of the reaction and the viscosity of the particle may be responsible for the very low yields of $C_{30}H_{48}O$ carbonyl products, further work is clearly needed to better understand peroxy radical chemistry in systems that form allylic alkyl radicals.

3.1.3. $C_{30}H_{50}(OH)_2$ Diol Product Isomers. Three TMS-derivatized $C_{30}H_{50}(OTMS)_2$ (m/z 588) diol isomers are detected at ∼1% and 10% [O_2]. The underivatized molecular formula of these diol isomers $C_{30}H_{50}(OH)_2$ corresponds to the addition of two O atoms and two H atoms to the squalene molecule. The formation of three isomers is consistent with the number of unique C═C double bonds in squalene. At ∼ 1% [O_2], the total mass concentration of $C_{30}H_{50}(OH)_2$ diol isomers reaches a maximum of ∼1810 $\mu g/m^3$ (OH exposure ∼1.5 × 10^{11} molecules cm^{-3} s, Figure 3c). At 10% [O_2], the total mass concentration of $C_{30}H_{50}(OH)_2$ diol isomers reaches a maximum of ∼1140 $\mu g/m^3$ (OH exposure ∼9.6 × 10^{10} molecules cm^{-3} s, Figure 3d). On the basis of the reaction mechanism shown in Figure 4, these $C_{30}H_{50}(OH)_2$ diol product isomers are formed by chain termination reactions between OH radicals and hydroxyalkyl radicals (R4) at ∼1% and 10% [O_2]. At high [O_2], $C_{30}H_{50}(OH)_2$ diols can also be formed by self- and cross-reactions of hydroxyperoxy radicals (R6) and H atom abstraction reactions by hydroxyalkoxy radicals (R8).

Figure S4a−c (Supporting Information) shows the VUV mass spectra of the three TMS-derivatized $C_{30}H_{50}(OTMS)_2$ diol isomers, and Figure S4d (Supporting Information) shows the relative abundance of the diol isomers. $C_{30}H_{50}(OTMS)_2$ diol isomers with OTMS groups on C2 and C3 of the squalene carbon backbone make up the majority (∼50%) of the structural isomers, suggesting that these diol isomers with hydroxyl groups located at the ends of the molecule are formed preferentially during the reaction. Ruehl et al.[4] also observed an overall enhancement in hydroxyl groups formed toward the ends of the molecule in the heterogeneous reaction of OH radicals with squalane aerosol. They attributed this to alkoxy radical sites located toward the ends of the molecule being more exposed to other molecules and are thus more likely to undergo intermolecular H atom abstraction. Analogous to the squalane reaction, it is possible that intermolecular H atom abstraction reactions by hydroxyalkoxy radicals in the squalene reaction (R8 in Figure 4) contribute to the observed distribution of diol product isomers.

3.1.4. Squalene Fragmentation Products. Figure 3 shows that there are larger quantities of particle phase fragmentation products formed during oxidation at 10% [O_2] relative to ∼1% [O_2]. The higher abundance of particle phase fragmentation products at 10% [O_2] is consistent with the reaction mechanism shown in Figure 4 and the previous study of the OH + squalene reaction,[25] both of which show that O_2 promotes fragmentation reactions and aerosol mass loss. These fragmentation reactions produce more volatile lower molecular weight oxygenated products via C−C bond scission along the carbon backbone. In some cases, the more volatile lower molecular weight oxygenated products may evaporate from the particle into the gas phase, leading to a detectable loss in aerosol mass.[10,12,15]

To identify which C−C bonds in squalene are most susceptible to bond cleavage during oxidation, the mass concentrations of the particle phase fragmentation products are plotted as a function of carbon number in Figure 6a. These

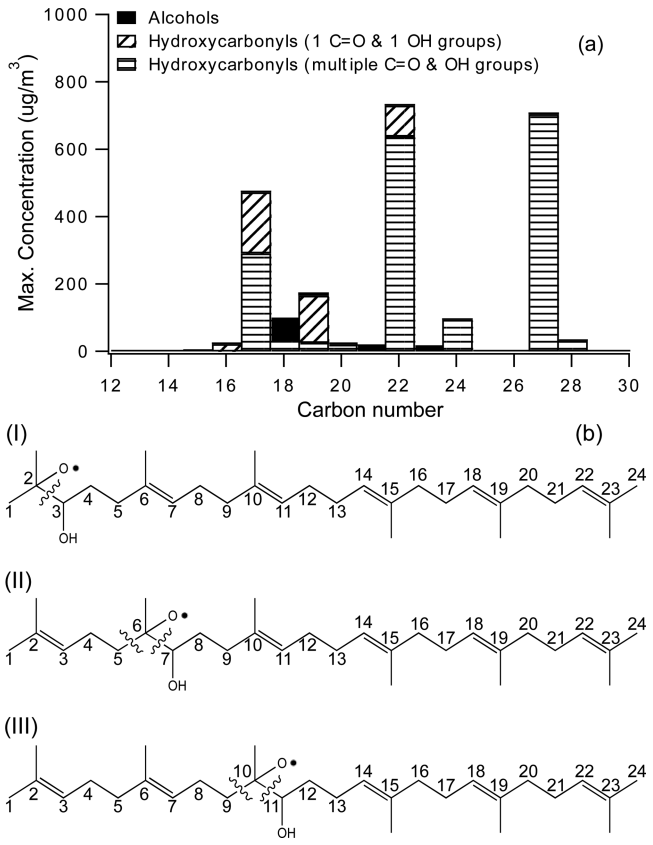

Figure 6. (a) Squalene fragmentation products as a function of carbon number at 10% [O_2] and an OH exposure of 7.32 × 10^{10} molecules cm^{-3} s (oxidation conditions at which maximum fragmentation product concentration is obtained). (b) Schematic of the C−C bonds in hydroxyalkoxy radicals that are most likely to undergo scission to form fragmentation products with carbon numbers (I) 27, (II) 22 and 24, and (III) 17 and 19. Also shown in part b are the labeled carbon atoms in the squalene carbon backbone.

classifications are made based on their retention times and parent molar masses. This analysis does not include fragmentation products with less than 10 carbon atoms since they are too volatile to be collected on filters. The analysis also does not include gas phase products (which are not measured) that may be formed during fragmentation reactions. However, previous studies of the squalene system[25] show that substantial aerosol mass loss occurs even at low OH exposures, indicating that the formation and subsequent loss of volatile lower molecular weight oxygenated products to the gas phase is an important reaction channel.

Figure 6a shows that the particle phase fragmentation products are made up of alcohols and hydroxycarbonyls. The majority of fragmentation products contain multiple hydroxyl (OH) and carbonyl (C═O) functional groups. The observation that most of the fragmentation products are multifunctional is expected, since these fragmentation products still have

dx.doi.org/10.1021/jp508378z | J. Phys. Chem. A 2014, 118, 11555−11571

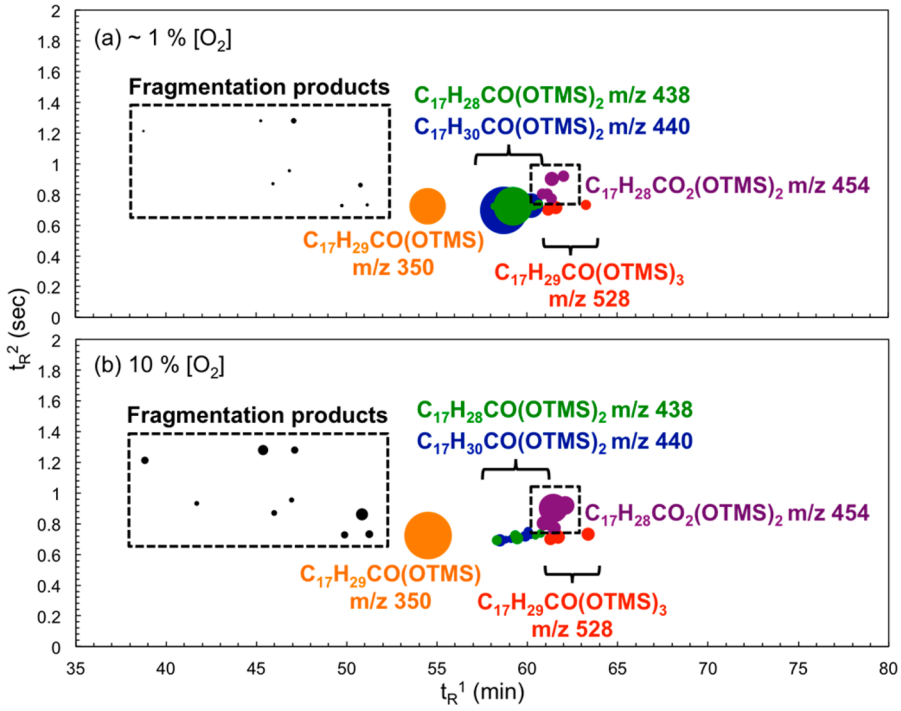

Figure 7. Relative abundance of linolenic acid and its oxidation products shown in GC × GC space at OH exposure =1.62 × 10^{11} molecules cm^{-3} s at (a) ~ 1% and (b) 10% [O_2]. The *x*-axis is the first dimension (t_R^1) and the *y*-axis is the second dimension (t_R^2) retention time. In panels a and b, each circle represents a single compound and its relative abundance is represented by the size of the circle. Derivatized linolenic acid $C_{17}H_{29}CO(OTMS)$ is the orange circle located at t_R^1 ~ 54.5 min and t_R^2 ~ 0.7 s. The oxidation products are separated into five groups by their chemical formulas and delineated with different colors: all fragmentation products (black); derivatized $C_{17}H_{28}CO(OTMS)_2$ alcohols (green); derivatized $C_{17}H_{30}CO(OTMS)_2$ alcohols (blue); derivatized $C_{17}H_{29}CO(OTMS)_3$ diols (red); derivatized $C_{17}H_{28}CO_2(OTMS)_2$ hydroxycarbonyls (purple).

C═C double bonds that are susceptible to further reaction with OH radicals and O_2. Majority of the fragmentation products have carbon number 20 and above. The measured abundance of products with carbon numbers less than 20 may be lower than their actual abundance (formed during the reaction) since some of these products may have evaporated from the particle prior to filter collection and analysis.

Figure 6a shows that the five most prominent carbon numbers of the fragmentation products, in order of decreasing abundance, are 22, 27, 17, 19, and 24. The large abundance of these fragmentation products can be explained by the dissociation of tertiary hydroxyalkoxy radicals (R10 in Figure 4). OH adds preferentially to the less substituted carbon of the C═C double bond (i.e., OH addition to C3, C7 and C11 of the squalene carbon backbone) during heterogeneous oxidation, leading to high yields of tertiary hydroxyalkoxy radicals at 10% [O_2]. In these tertiary hydroxyalkoxy radicals, the alkoxy radical sites are located at C2, C6 and C10 of the squalene carbon backbone (shown in Figure 6b). Previous studies[4,7−10,12,13,30,31] have shown that bond cleavage occurs at C−C bonds adjacent to the alkoxy radical site. Here cleavage of the C2−C3 bond in the squalene carbon backbone (which is adjacent to the alkoxy radical at C2 of the squalene carbon backbone) leads to the formation of fragmentation products with carbon number 27 (I in Figure 6b). Similarly, cleavage of the C5−C6 and C6−C7 bonds in the squalene carbon backbone produce fragmentation products with carbon numbers 24 and 22, respectively (II in Figure 6b). Cleavage of the C9−C10 and C10−C11 bonds in the squalene carbon backbone produce fragmentation products with carbon numbers 19 and 17, respectively (III in Figure 6b).

Approximately 78% of the total fragmentation product mass concentration consists of products with carbon numbers 17, 22 and 27, indicating that the C10−C11, C6−C7, and C2−C3 bonds in the squalene carbon backbone are most susceptible to cleavage. This suggests that hydroxyalkoxy radical dissociation occurs primarily at C−C bonds that are adjacent to both the alkoxy radical site and hydroxyl group. The close proximity of the hydroxyl group to the alkoxy radical site likely increases the rates of C2−C3, C6−C7, and C10−C11 bond cleavage. Quantum chemical calculations[37] on barrier heights and enthalpies for tertiary hydroxyalkoxy radical dissociation (shown and described in Figure S5 in the Supporting Information) support this hypothesis. While the reaction energy is largely consistent between the three fragmentation pathways, cleavage of the C−C bond adjacent to both the alkoxy radical site and hydroxyl group has the lowest barrier height. This observation is also consistent with previous aerosol oxidation studies, which showed that the presence of oxygenated functional groups (e.g., alcohols and carbonyls) may increase the rates of alkoxy dissociation reactions.[10,12,15]

3.2. Linolenic Acid Oxidation Product Analysis.

3.2.1. Linolenic Acid GC × GC Chromatogram. Figure 7 shows the distribution and relative abundance of particle phase linolenic acid oxidation products in GC × GC space at an OH exposure of 1.6 × 10^{11} molecules cm^{-3} s for ~1% and 10% [O_2] (Figure 7, part a and b, respectively). Each circle signifies a single compound and its relative abundance is represented by the size of the circle. TMS-derivatized linolenic acid $C_{17}H_{29}CO$-(OTMS) (*m*/*z* 350, shown in orange in Figure 7) elutes at t_R^1 ~ 54.5 min and t_R^2 ~ 0.7 s. The fragmentation products (shown in black in Figure 7) have carbon numbers less than 18

dx.doi.org/10.1021/jp508378z | J. Phys. Chem. A 2014, 118, 11555−11571

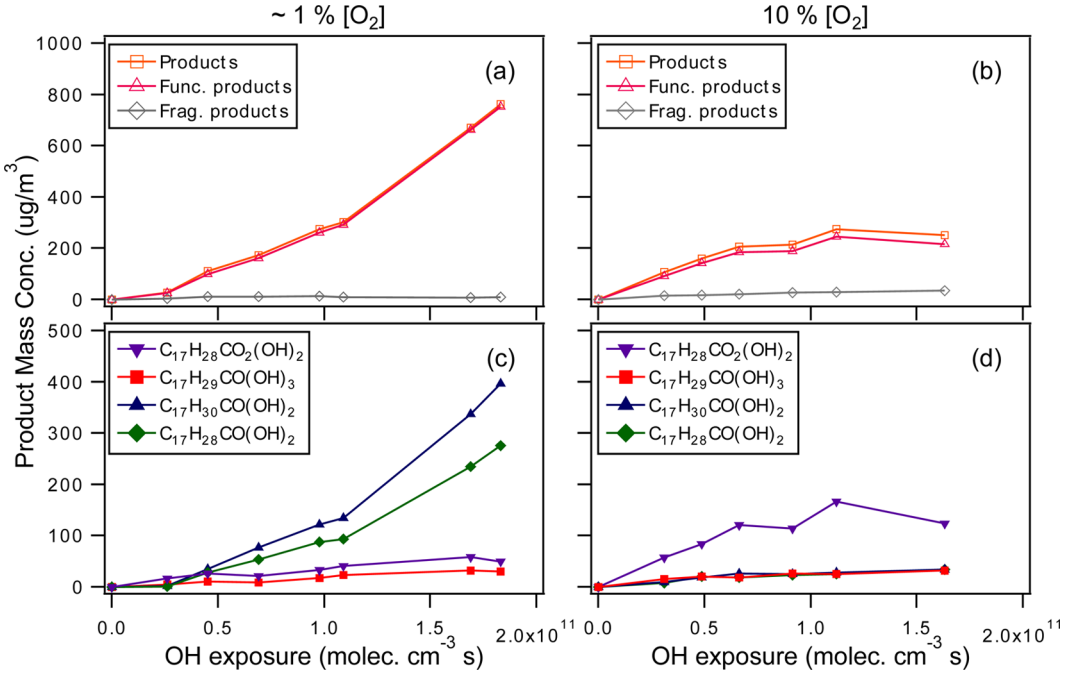

Figure 8. Total mass concentrations of linolenic acid oxidation products, functionalization products and fragmentation products as a function of OH exposure at (a) ~ 1% [O_2], and (b) 10% [O_2]. Total mass concentrations of $C_{17}H_{28}CO(OH)_2$ alcohol, $C_{17}H_{30}CO(OH)_2$ alcohol, $C_{17}H_{29}CO(OH)_3$ diol and $C_{17}H_{28}CO_2(OH)_2$ hydroxycarbonyl products as a function of OH exposure at (c) ~ 1% [O_2], and (d) 10% [O_2].

and elute at earlier t_R^1 than linolenic acid. The functionalization products (which elute at later t_R^1 than linolenic acid) are grouped based on their molecular formulas.

Two groups of TMS-derivatized alcohol products are detected as functionalization products: $C_{17}H_{28}CO(OTMS)_2$ (m/z 438, shown in green in Figure 7) and $C_{17}H_{30}CO(OTMS)_2$ (m/z 440, shown in blue in Figure 7). Ten $C_{17}H_{28}CO(OTMS)_2$ alcohol isomers are detected at ~1% [O_2] (Figure 7a), while only five $C_{17}H_{28}CO(OTMS)_2$ isomers are detected 10% [O_2] (Figure 7b), indicating that [O_2] has a considerable influence on the formation of these alcohol isomers. These $C_{17}H_{28}CO(OTMS)_2$ alcohol isomers elute at t_R^2 ~ 0.7 s with t_R^1 from ~58 to 61 min at both ~1% and 10% [O_2]. At both ~1% and 10% [O_2], six $C_{17}H_{30}CO(OTMS)_2$ isomers are detected at t_R^2 ~ 0.7 s with t_R^1 from ~58 to 61 min. Three TMS-derivatized diol isomers $C_{17}H_{29}CO(OTMS)_3$ (m/z 528, shown in red in Figure 7) are detected at t_R^2 ~ 0.7 s with t_R^1 from ~61 to 64 min, while six TMS-derivatized hydroxycarbonyl isomers $C_{17}H_{28}CO_2(OTMS)_2$ (m/z 454, shown in purple in Figure 7) are detected at t_R^1 from ~61 to 64 min and t_R^2 from ~0.8 to 0.9 s. MSTFA derivatization decreases the polarities of the TMS-derivatized linolenic acid and its alcohol and diol functionalization products, causing them to have shorter t_R^2 than the TMS-derivatized hydroxycarbonyl functionalization products.

The mass concentrations of particle phase linolenic acid products are quantified using external standards. Parts a and b of Figure 8 show the total mass concentrations of detected oxidation products, functionalization products and fragmentation products as a function of OH exposure at ~1% and 10% [O_2], respectively. Error bars for the oxidation product mass concentrations are not shown since there is some uncertainty on how the detection efficiencies of the external standards differ from that of the products.

A comparison of the mass concentrations of detected squalene and linolenic acid oxidation products (Figures 3 and 8, respectively) suggests that the total abundance of linolenic acid products that are detected is significantly smaller than the squalene products. However, this may not be the case since the external standards used in this study have only one or two oxygenated functional groups, which may not be suitable for accurate quantification of highly oxygenated linolenic acid products due to differing response factors. The majority of linolenic acid products have three or more oxygenated functional groups, while most of the squalene products only have one or two oxygenated functional groups. Highly oxygenated compounds (with three or more oxygenated functional groups) may also have lower GC column transfer efficiencies.[13] While these limitations prevent the accurate quantification of linolenic acid oxidation products, it is still useful to quantify and compare the linolenic acid products at ~1% and 10% [O_2] to gain insights into the role of [O_2] on the product formation chemistry. Because of the presence of a contaminant (linoleic acid, which is present as an impurity in the linolenic acid solution used to generate aerosol) that coelutes with the TMS-derivatized linolenic acid, the effective uptake coefficient for linolenic acid (γ_{OH}^{LNA}) could not be determined from the EI-MS measurements. However, previous kinetic studies of the linolenic acid reaction[24] reported that γ_{OH}^{LNA} decreases when [O_2] increases, implying that O_2, unlike for the squalene reaction, promotes chain termination.

Figure 8a shows that at ~1% [O_2] the total mass concentration of detected oxidation products increases with OH exposure. The total mass concentration of detected oxidation products reaches a maximum value of ~760 $\mu g/m^3$ at an OH exposure of ~1.8 × 10^{11} molecules cm^{-3} s. Approximately 95% of the observed products are functionalization products, and approximately 5% are fragmentation products.

Figure 8b shows that at 10% [O_2] the total mass concentration of detected oxidation products increases and reaches a maximum value of ~280 $\mu g/m^3$ at an OH exposure of

dx.doi.org/10.1021/jp508378z | J. Phys. Chem. A 2014, 118, 11555−11571

~1.1 × 10^{11} molecules cm^{-3} s. Approximately 88% of the observed oxidation products are functionalization products, and approximately 12% are fragmentation products. The large abundance of functionalization products accompanied by very low yields of fragmentation products at ~1% and 10% [O_2] indicate that functionalization pathways play more prominent roles in linolenic acid oxidation irrespective of [O_2] (relative to squalene oxidation).

The total mass concentration of oxidation products is larger at ~1% [O_2] than at 10% [O_2]. The differences in the total mass concentration of oxidation products can be attributed to differences in the functionalization product distribution at ~1% and 10% [O_2]. For example, 10 TMS-derivatized $C_{18}H_{28}O$-$(OTMS)_2$ alcohol isomers are detected at ~1% [O_2], while only five such alcohol isomers are detected 10% [O_2]. This suggests that [O_2] controls the formation of these alcohol products and consequently, the contribution of these alcohol products to the total mass concentration of oxidation products. The role that O_2 plays in controlling the distribution of functionalization products will be discussed further in sections 3.2.4 and 3.2.3.

The functionalization products are composed of TMS-derivatized $C_{17}H_{28}CO(OTMS)_2$, $C_{17}H_{30}CO(OTMS)_2$, $C_{17}H_{29}CO(OTMS)_3$, and $C_{17}H_{28}CO_2(OTMS)_2$ product isomers. The underivatized molecular formulas of these products (obtained by substituting the "TMS" group with a H atom) are $C_{17}H_{28}CO(OH)_2$, $C_{17}H_{30}CO(OH)_2$, $C_{17}H_{29}CO(OH)_3$, and $C_{17}H_{28}CO_2(OH)_2$. Previous kinetic studies[24] indicate that these are all first generation functionalization products. Figures 8c and 8d show the evolution of $C_{17}H_{28}CO(OH)_2$, $C_{17}H_{30}CO$-$(OH)_2$, $C_{17}H_{29}CO(OH)_3$, and $C_{17}H_{28}CO_2(OH)_2$ mass concentrations as a function of OH exposure at ~1% and 10% [O_2], respectively. At ~ 1% [O_2], $C_{17}H_{28}CO(OH)_2$, $C_{17}H_{30}CO(OH)_2$, $C_{17}H_{29}CO(OH)_3$, and $C_{17}H_{28}CO_2(OH)_2$ make up approximately 29%, 41%, 9% and 21% of the total mass concentration of observed functionalization products, respectively (Figure 8c). At 10% [O_2], $C_{17}H_{28}CO(OH)_2$, $C_{17}H_{30}CO(OH)_2$, $C_{17}H_{29}CO(OH)_3$, and $C_{17}H_{28}CO_2(OH)_2$ make up approximately 12%, 13%, 13%, and 62% of the total mass concentration of observed functionalization products, respectively (Figure 8d).

The formation of first generation $C_{17}H_{28}CO(OH)_2$, $C_{17}H_{30}CO(OH)_2$, $C_{17}H_{29}CO(OH)_3$, and $C_{17}H_{28}CO_2(OH)_2$ functionalization products can be explained by the reaction mechanism proposed previously by Nah et al.[24] Figure 9 shows this reaction mechanism for the OH-initiated oxidation of linolenic acid aerosol. Similar to the OH + squalene reaction,[25] the OH + linolenic acid reaction is initiated by OH addition to the C=C double bond. For clarity, the derivatized and underivatized molecular formulas of the products are also shown. Product isomers are analyzed in sections 3.2.4 − 3.2.4 within the context of the reaction mechanism.

Similar to the squalene reaction, we see no evidence of organic peroxide products formed from hydroxyalkyl/alkyl radical + hydroxyperoxy/peroxy radical (R + RO_2), hydroxyalkyl/alkyl radical + hydroperoxyl radical (R + HO_2) and hydroxyperoxy/peroxy radical + hydroperoxyl radical (RO_2 + HO_2) reactions. Therefore, these chain termination reactions appear to be minor channels, within out ability to detect these products, in the linolenic acid reaction, and are not included in the reaction mechanism shown in Figure 9. Carbonyls, which can be formed from the reaction of alkoxy radicals with HO_2 radicals, are also not detected in the GC × GC chromatograms.

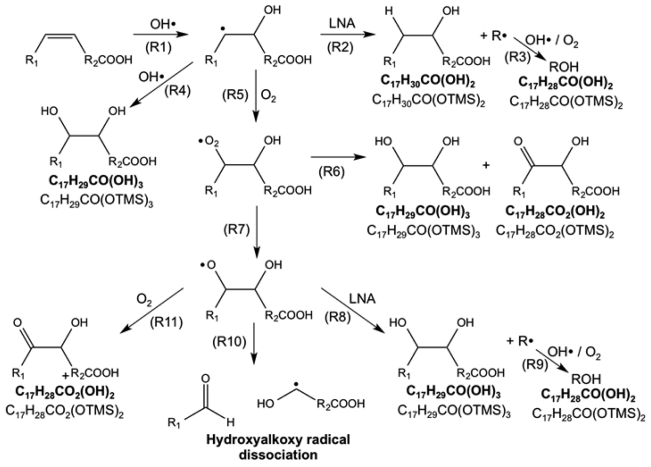

Figure 9. Reaction mechanism for the OH-initiated oxidation of linolenic acid (LNA) aerosol. R• represents the generic alkyl radical formed by the abstraction of a H atom from a linolenic acid molecule. The underivatized (bold text) and derivatized (regular text) molecular formulas of the detected first generation functionalization products are also shown.

This suggests that they are likely minor channels in the linolenic acid reaction, and are therefore not included in the reaction mechanism shown in Figure 9.

3.2.2. $C_{17}H_{30}CO(OTMS)_2$ and $C_{17}H_{28}CO(OH)_2$ Alcohol Product Isomers. Six TMS-derivatized $C_{17}H_{30}CO(OTMS)_2$ alcohol isomers are detected at both ~1% and 10% [O_2]. The underivatized molecular formula of these alcohol isomers $C_{17}H_{30}CO(OH)_2$ indicates that one O atom and two H atoms are added to the linolenic acid molecule. These $C_{17}H_{30}CO$-$(OH)_2$ alcohol product isomers are formed by the chain reaction where a H atom is abstracted from a neighboring linolenic acid molecule by the hydroxyalkyl radical (R2 in Figure 9). The detection of six TMS-derivatized $C_{17}H_{30}CO$-$(OTMS)_2$ alcohol isomers can be explained by the molecular structure of linolenic acid. Linolenic acid is a linear molecule with six carbon sites that OH can add to form secondary hydroxyalkyl radicals. Since OH addition is predicted to be approximately equally rapid at either of the carbons in the C=C double bonds of linolenic acid,[19] six different secondary hydroxyalkyl radicals are expected to be formed, resulting in the formation of six $C_{17}H_{30}CO(OH)_2$ alcohol product isomers. Since the mass spectra of these six isomers contain similar fragment ions, we are not able to assign structural isomers.

At ~ 1% [O_2], the total mass concentration of $C_{17}H_{30}CO$-$(OH)_2$ alcohol isomers reaches a maximum of ~400 $\mu g/m^3$ (OH exposure ~1.8 × 10^{11} molecules cm^{-3} s, Figure 8c). At 10% [O_2], the total mass concentration of $C_{17}H_{30}CO(OH)_2$ alcohol isomers reaches a maximum of ~30 $\mu g/m^3$ (OH exposure ~1.6 × 10^{11} molecules cm^{-3} s, Figure 8d). Thus, the total abundance of these alcohol isomer products is approximately 13 times larger at ~1% [O_2] compared to 10% [O_2], indicating that O_2 suppresses the formation of $C_{17}H_{30}CO(OH)_2$ products. This suggests that the formation of secondary hydroxyperoxy radicals (R5 in Figure 9) becomes the dominant reaction pathway for hydroxyalkyl radicals at high [O_2], effectively slowing down the chain propagation reaction that produces the $C_{17}H_{30}CO(OTMS)_2$ alcohol products (R2 in Figure 9).

Ten TMS-derivatized $C_{17}H_{28}CO(OTMS)_2$ alcohol isomers are detected at ~1% [O_2], while only five such alcohol isomers

dx.doi.org/10.1021/jp508378z | J. Phys. Chem. A 2014, 118, 11555−11571

are detected at 10% [O_2]. The underivatized molecular formula of these alcohol isomers $C_{17}H_{28}CO(OH)_2$ corresponds to the addition of one O atom to the linolenic acid molecule. At ~ 1% [O_2] the total mass concentration of $C_{17}H_{28}CO(OH)_2$ alcohol isomers reaches a maximum of ~280 $\mu g/m^3$ (OH exposure ~1.8×10^{11} molecules cm^{-3} s, Figure 8c). At 10% [O_2] the total mass concentration of $C_{17}H_{28}CO(OH)_2$ alcohol isomers reaches a maximum of ~30 $\mu g/m^3$ (OH exposure ~1.6×10^{11} molecules cm^{-3} s, Figure 8d). These $C_{17}H_{28}CO(OH)_2$ alcohol isomers can be formed by the reaction of alkyl (R) radicals (formed by H atom abstraction by OH, hydroxyalkyl and hydroxyalkoxy radicals) with O_2 and OH radicals (R3 and R9 in Figure 9). Since the mass spectra of these $C_{17}H_{28}CO(OTMS)_2$ alcohol isomers contain similar fragment ions, we are not able to assign structural isomers.

The decrease in the number and total mass concentration of these alcohol product isomers with increasing [O_2] can be explained by the reaction mechanism shown in Figure 9. At low [O_2], secondary hydroxyalkyl radicals can propagate the particle-phase secondary chain chemistry by abstracting a H atom from a neighboring linolenic acid molecule to form R radicals (R2), which can react with O_2 and OH radicals to form $C_{17}H_{28}CO(OH)_2$ alcohol products (R3). When increasing amounts of O_2 are added to the reaction, the secondary hydroxyalkyl radicals can react instead with O_2 to form secondary hydroxyperoxy radicals (R5), effectively slowing down the formation of R radicals via R2 and suppressing the formation of these $C_{17}H_{28}CO(OH)_2$ alcohol products from R3. The formation of R radicals from H atom abstraction reactions by hydroxyalkoxy radicals (R8) is a minor channel at high [O_2] since low yields of hydroxyalkoxy radicals are formed from self- and cross-reactions of hydroxyperoxy radicals (R7).

The detection of ten TMS-derivatized $C_{17}H_{28}CO(OTMS)_2$ alcohol isomers at ~1% [O_2] is consistent with the number of allylic H atoms in the linolenic acid molecule. While linolenic acid has 23 H atoms in $C(sp^3)$−H bonds (along the carbon backbone) available for H abstraction, there are only 4 allylic $C(sp^3)$-H sites. Allylic $C(sp^3)$−H bonds have significantly lower bond energies than nonallylic $C(sp^3)$−H bonds.[35,36] Therefore, the rate constants for H atom abstraction reactions may be higher at these 4 sites. The allylic H atoms of linolenic acid are located at C8, C11, C14 and C17 of the linolenic acid carbon backbone (shown in Figure S6a in the Supporting Information). The allylic R radicals formed from H atom abstraction reactions are resonance stabilized. A total of 10 resonance-stabilized allylic R radicals can be formed (shown in Figure S6b in the Supporting Information), which results in the formation of 10 $C_{17}H_{28}CO(OH)_2$ alcohol products at ~1% [O_2].

Previous studies[28−32] have shown that R radicals can react with O_2 to form peroxy radicals, which self- and cross-react with other peroxy and hydroxyperoxy radicals to form particle phase products with one hydroxyl group ($C_{17}H_{28}CO(OH)_2$) or one carbonyl group ($C_{18}H_{28}O_3$). Similar to the squalene reaction, $C_{18}H_{28}O_3$ carbonyls are not detected, indicating that they are minor reaction products. Analogous to the squalene reaction, while it is possible that the temperature of the reaction and the viscosity of the linolenic acid particle are responsible for the very low yields of $C_{18}H_{28}O_3$ carbonyl products, better understanding of the oxidation chemistry at allylic R radical sites is clearly needed.

3.2.3. $C_{17}H_{28}CO_2(OH)_2$ Hydroxycarbonyl and $C_{17}H_{29}CO(OH)_3$ Diol Product Isomers. Six TMS-derivatized $C_{17}H_{28}CO_2(OTMS)_2$ hydroxycarbonyl product isomers are detected at both ~1% and 10% [O_2]. The underivatized molecular formula of these hydroxycarbonyl isomers is $C_{17}H_{28}CO_2(OH)_2$. Figure S7a−f (Supporting Information) shows the VUV mass spectra of the six TMS-derivatized $C_{17}H_{28}CO_2(OTMS)_2$ hydroxycarbonyl product isomers, while Figure S7g (Supporting Information) shows the relative abundance of the six hydroxycarbonyl isomers. $C_{17}H_{28}CO_2(OTMS)_2$ hydroxycarbonyl isomers with the OTMS group positioned at C12 and carbonyl group positioned at C13 make up the majority (~30%) of the structural isomers. This suggests that $C_{17}H_{28}CO_2(OH)_2$ hydroxycarbonyl isomers with the hydroxyl and carbonyl groups at C12 and C13, respectively, are formed preferentially (compared to the other five isomers) during the reaction.

To determine more generally which C=C double bonds in linolenic acid (i.e., C15=C16 vs C12=C13 vs C9=C10) are most susceptible to the addition of hydroxyl and carbonyl groups, the relative abundances of $C_{17}H_{28}CO_2(OH)_2$ hydroxycarbonyl isomers are plotted as a function of carbon atom position along the linolenic acid backbone in Figure 10. There

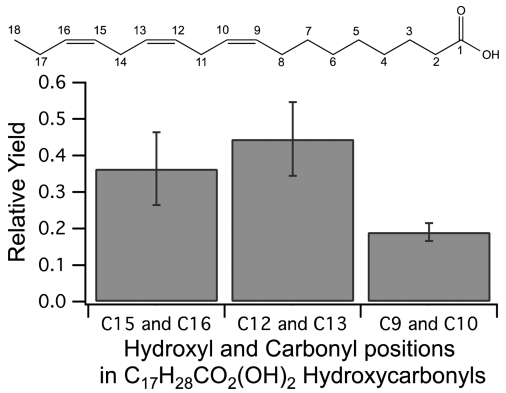

Figure 10. Distribution of $C_{17}H_{28}CO_2(OH)_2$ hydroxycarbonyl product isomers as a function of carbon atom position along the linolenic acid backbone. Error bars represent the different fractions of positional isomers under different OH exposure conditions. Also shown are the labeled carbon atoms in the linolenic acid carbon backbone.

is an enhancement in the addition of hydroxyl and carbonyl groups to C=C double bonds located at the terminus of the linolenic acid molecule (i.e., C15=C16 and C12=C13 double bonds). Isomers formed from the addition of hydroxyl and carbonyl groups to the C15=C16 and C12=C13 double bonds make up ~36% and 45% of the total hydroxycarbonyl mass concentration, respectively. One possible explanation for the observed product distribution is that particle phase linolenic acid molecules are oriented perpendicular to the particle surface, with the C15=C16 and C12=C13 double bonds preferentially exposed to (and consequently susceptible to reaction with) gas phase OH radicals and O_2. This proposed molecular orientation of linolenic acid molecules at the particle surface is similar to that proposed previously by Hearn et al.[41] of oleic acid (linear C_{18} carboxylic acid with one C=C double bond) molecules at the particle surface.

At ~ 1% [O_2], the total mass concentration of $C_{17}H_{28}CO_2(OH)_2$ hydroxycarbonyl isomers reaches a maximum of ~60 $\mu g/m^3$ (OH exposure ~1.7×10^{11} molecules cm^{-3} s, Figure 8c). At 10% [O_2], the total mass concentration

dx.doi.org/10.1021/jp508378z | J. Phys. Chem. A 2014, 118, 11555−11571

of $C_{17}H_{28}CO_2(OH)_2$ hydroxycarbonyl isomers reaches a maximum of ~170 $\mu g/m^3$ (OH exposure ~1.1 × 10^{11} molecules cm^{-3} s, Figure 8d). Since $C_{17}H_{28}CO_2(OH)_2$ hydroxycarbonyls make up the majority (~62%) of the functionalization products at 10% $[O_2]$ but are minor (~21%) functionalization products at ~1% $[O_2]$, this indicates that O_2 promotes the formation of these hydroxycarbonyl products. On the basis of the reaction mechanism shown in Figure 9, $C_{17}H_{28}CO_2(OH)_2$ hydroxycarbonyl products are formed from self- and cross-reactions of secondary hydroxyperoxy radicals (R6) and the reaction of O_2 with hydroxyalkoxy radicals (R11). At low $[O_2]$, the formation rates of secondary hydroxyperoxy (R5) and hydroxyalkoxy radicals (R7) are slowed, leading to low yields of hydroxycarbonyl products. Conversely secondary hydroxyperoxy and hydroxyalkoxy radicals are formed in high yields at high $[O_2]$. The secondary hydroxyperoxy radicals can then self- and cross-react via the Russell and Bennett−Summers mechanisms[25−29] (R6) and the secondary hydroxyalkoxy radicals can react with O_2 (R11) to form $C_{17}H_{28}CO_2(OH)_2$ hydroxycarbonyl products.

The importance of hydroxycarbonyl product formation at high $[O_2]$ is consistent with previous measurements of γ_{OH}^{LNA}. Nah et al.[24] showed that γ_{OH}^{LNA} decreases when $[O_2]$ increases (6.21 ± 0.17 at ~0% $[O_2]$ vs 5.73 ± 0.14 at 10% $[O_2]$), implying that chain termination reactions become more prominent at higher $[O_2]$. This is consistent with the reaction mechanism shown in Figure 9, which shows that secondary hydroxyalkyl radicals propagate the particle-phase secondary chain chemistry at low $[O_2]$ by abstracting a H atom from the neighboring linolenic acid molecules (R2). When increasing amounts of O_2 are added to the reaction, the secondary hydroxyalkyl radicals can react with O_2 to form secondary hydroxyperoxy radicals (R5) instead. These secondary hydroxyperoxy radicals can then self- and cross-react via the Russell and Bennett−Summers mechanisms[28−32] (R6) to form stable oxygenated products (via chain termination). This slows the radical chain chemistry in the particle, causing a decrease in γ_{OH}^{LNA} with increasing $[O_2]$. It should be pointed out that the γ_{OH}^{LNA} vs $[O_2]$ trend is strongly influenced by the ratio of the hydroxyalkyl radical + linolenic acid (R2) reaction rate to the hydroxyalkyl radical + O_2 (R5) reaction rate. Preliminary results suggest that the ratio has to be ≥10 to obtain the observed γ_{OH}^{LNA} vs $[O_2]$ trend, and it can change based on the reaction rates of the other reaction pathways. Detailed modeling of the branching ratios of the different pathways responsible for the measured effective uptake coefficients and product distributions will be presented in an upcoming publication.

In addition to the $C_{17}H_{28}CO_2(OH)_2$ hydroxycarbonyl products, self- and cross-reactions of secondary hydroxyperoxy radicals (R6 in Figure 9) also produce $C_{17}H_{29}CO(OH)_3$ diols. $C_{17}H_{29}CO(OH)_3$ diols (detected as $C_{17}H_{29}CO(OTMS)_3$) can also be formed by the reaction of hydroxyalkyl radicals with OH (R4 in Figure 9), and H atom abstraction reaction by secondary hydroxyalkoxy radicals (R8 in Figure 9). Figure S1b−d (Supporting Information) shows the VUV mass spectra of the three TMS-derivatized $C_{17}H_{29}CO(OTMS)_3$ diol product isomers, while Figure S1e (Supporting Information) shows the relative abundance of the three diol isomers. The relative abundances of the three diol isomers are approximately the same (~33% each), suggesting that these diol isomers are formed at equal rates. This result differs from that of the hydroxycarbonyl isomers, which show that hydroxyl and carbonyl groups are added preferentially to C=C double bonds located at the terminus of the linolenic acid molecule (Figure 10). It is currently unclear why this is the case and should be an area of focus for further investigation.

At ~ 1% $[O_2]$ the total mass concentration of $C_{17}H_{29}CO(OH)_3$ diol isomers increases and reaches a maximum of ~30 $\mu g/m^3$ (OH exposure ~1.7 × 10^{11} molecules cm^{-3} s, Figure 8c), and is ~9% of the total mass concentration of functionalization products. At 10% $[O_2]$ the total mass concentration of $C_{17}H_{29}CO(OH)_3$ diol isomers increases and reaches a maximum of ~30 $\mu g/m^3$ (OH exposure ~1.1 × 10^{11} molecules cm^{-3} s, Figure 8d), and is ~13% of the total mass concentration of functionalization products. This indicates that, unlike the hydroxycarbonyl products, the total mass concentration of diol products appears to be independent of $[O_2]$ in the reactor.

One possible explanation for the relatively low diol product mass concentrations at 10% $[O_2]$ is that hydroxycarbonyls are formed in excess of diol products in the self- and cross-reactions of secondary hydroxyperoxy radicals (R6 in Figure 9), consistent with Hearn et al.[28] who also observed excess carbonyl formation (relative to alcohols) in the Cl oxidation of dioctyl sebacate aerosol. They attributed this to the importance of the Bennett−Summers mechanism at high $[O_2]$. Unlike the Russell mechanism[26−28] that produces equal quantities of alcohols and carbonyls in peroxy radical self- and cross-reactions, only carbonyls are produced in the Bennett−Summers mechanism.[28,30−32]

The excess formation of hydroxycarbonyl products (relative to diol products) at high $[O_2]$ can also be attributed to the fact that the H atom abstraction reaction by secondary hydroxyalkoxy radicals (R8 in Figure 9) is a minor reaction channel at high $[O_2]$. As discussed previously by Nah et al.,[25] low yields of hydroxyalkoxy radicals are formed from secondary hydroxyperoxy radical self- and cross-reactions (R7 in Figure 9) at high $[O_2]$. This is consistent with the results of Docherty et al.,[42] which showed that alkoxy radical formation is a minor reaction pathway in the NO_3 oxidation of oleic acid aerosol.

3.2.4. Linolenic Acid Fragmentation Products. At ~ 1% $[O_2]$ the total mass concentration of detected fragmentation products reaches a maximum of ~10 $\mu g/m^3$ (OH exposure ~9.8 × 10^{10} molecules cm^{-3} s, Figure 8a). At 10% $[O_2]$ the total detected fragmentation product mass concentration reaches a maximum of ~30 $\mu g/m^3$ (OH exposure ~1.6 × 10^{11} molecules cm^{-3} s, Figure 8b). Fragmentation products makes up approximately 5 and 12% of the total mass concentration of oxidation products at ~1% and 10% $[O_2]$, respectively. The formation of gas phase fragmentation products is expected to be a minor channel as evident by the small detectible loss in aerosol mass measured previously by Nah et al.[24] Therefore, the very low yields of fragmentation products at ~1% and 10% $[O_2]$ indicate that, unlike squalene, fragmentation is only a minor channel in linolenic acid oxidation.

The minor role that fragmentation plays in linolenic acid oxidation can be explained by the reaction mechanism shown in Figure 9. The only route for fragmentation product formation is via hydroxyalkoxy radical dissociation (R10). At ~ 1% $[O_2]$, pathway R10 is effectively suppressed since hydroxyperoxy radicals (and consequently hydroxyalkoxy radicals) are formed in low abundance. At 10% $[O_2]$, secondary hydroxyperoxy radicals are formed in high yields. These secondary

hydroxyperoxy radicals can preferentially self- and cross-react via the Russell and Bennett−Summers mechanisms[28−32] (R6) to form terminal stable oxygenated products (i.e., chain termination). Even though secondary hydroxyalkoxy radicals can be formed from self-and cross-reactions of secondary hydroxyperoxy radicals (R7), the low abundance of particle phase fragmentation products at 10% [O_2] indicates that pathway R7 is a minor reaction channel. This is consistent with the previous study of the OH + linoleic acid reaction,[24] which showed that the average number of C atoms in the linoleic acid molecule stays roughly constant at 18 during oxidation at 10% [O_2], indicating little C−C bond cleavage. These measurements are also consistent with that by Docherty et al.[42] in the NO_3 oxidation of oleic acid aerosol, which showed that the formation of oxygenated products is a major reaction pathway while the formation of alkoxy radicals is of minimal importance.

4. CONCLUSIONS

The oxidation products from two model reaction systems, OH + squalene ($C_{30}H_{50}$, a branched alkene with six C═C double bonds) and OH + linolenic acid ($C_{18}H_{30}O_2$, a linear carboxylic acid with three C═C double bonds), are analyzed to investigate the effect of molecular structure (branched vs linear) on product formation in the heterogeneous OH-initiated oxidation of unsaturated organic aerosol. The oxidation products of squalene and linolenic acid are identified and quantified using two-dimensional gas chromatography−mass spectrometry. In both squalene and linolenic acid oxidation, the reaction is initiated by OH addition to the C═C double bonds to form hydroxyalkyl radicals. Allylic alkyl radicals, formed from H abstraction reactions by hydroxyalkyl radicals, play important roles in particle-phase secondary chain chemistry and product distributions. Oxidation products arising from secondary chain reactions are detected in large abundance in both reaction systems, indicating that secondary chain chemistry plays a major role in the heterogeneous oxidation of unsaturated organic aerosol.

Functionalization products are the dominant products in squalene oxidation at ∼1% [O_2], with 89% and 11% of the total observed oxidation product mass concentration being functionalization and fragmentation products, respectively. $C_{30}H_{49}OH$ alcohols, $C_{30}H_{51}OH$ alcohols and $C_{30}H_{50}(OH)_2$ diols make up 46%, 22% and 32% of the observed functionalization products, respectively. At 10% [O_2], the total mass concentration of functionalization products is approximately equal to the fragmentation products. $C_{30}H_{49}OH$ alcohols, $C_{30}H_{51}OH$ alcohols and $C_{30}H_{50}(OH)_2$ diols make up 47%, 11% and 42% of the observed functionalization products, respectively. Approximately 90% and 80% of the original squalene mass concentration can be accounted for (by particle phase products and unreacted squalene) over the course of the reaction at ∼1% and 10% [O_2], respectively. Analysis of squalene functionalization products reveals that oxidation is initiated predominantly by OH addition to the less substituted carbon of the C═C double bond. Functionalization products originating from OH addition to the more substituted carbon of the C═C double bond are not observed, indicating that it is a minor reaction channel. The large abundance of squalene fragmentation products at 10% [O_2] is attributed to the formation and dissociation of tertiary hydroxyalkoxy radicals in the presence of O_2. Analysis of squalene fragmentation products indicates that hydroxyalkoxy radical dissociation occurs primarily at C−C bonds that are adjacent to both the alkoxy radical site and hydroxyl group.

In contrast to squalene, functionalization products are the dominant products in linolenic acid aerosol oxidation at both ∼1% and 10% [O_2]. At ∼ 1% [O_2], approximately 95% and 5% of the total observed oxidation product mass concentration are functionalization and fragmentation products, respectively. At 10% [O_2], approximately 88% and 12% of the total observed oxidation product mass concentration are functionalization and fragmentation products, respectively. At ∼ 1% [O_2], $C_{17}H_{28}CO(OH)_2$ alcohols, $C_{17}H_{30}CO(OH)_2$ alcohols, $C_{17}H_{29}CO(OH)_3$ diols and $C_{17}H_{28}CO_2(OH)_2$ hydroxycarbonyls make up 29%, 41%, 9% and 21% of the total observed functionalization products, respectively. At 10% [O_2], $C_{17}H_{28}CO(OH)_2$ alcohols, $C_{17}H_{30}CO(OH)_2$ alcohols, $C_{17}H_{29}CO(OH)_3$ diols, and $C_{17}H_{28}CO_2(OH)_2$ hydroxycarbonyls make up 12%, 13%, 13%, and 62% of the total observed functionalization products, respectively. The significantly lower yields of linolenic acid fragmentation products indicate that fragmentation is a minor reaction channel irrespective of [O_2]. Analysis of linolenic acid functionalization products shows that oxidation is initiated by OH addition to either of the carbons in the C═C double bonds, leading to the formation of secondary hydroxyalkyl radicals. The distribution of linolenic acid functionalization products is governed by [O_2], suggesting that O_2 controls the functionalization pathways taken by the secondary hydroxyalkyl radical intermediate.

In summary, the differences in the squalene and linolenic acid product distributions can be understood by comparing the roles that the hydroxyalkyl, hydroxyperoxy and hydroxyalkoxy radical intermediates play in the two reaction systems. At ∼ 1% [O_2] (i.e., low [O_2]), hydroxyalkyl radicals (formed by OH addition to the C═C double bonds) react mainly with OH radicals to form diols, and with neighboring squalene and linolenic acid molecules to form alcohols. In both reaction systems, the formation of hydroxyperoxy radicals is suppressed at ∼1% [O_2] due to the low concentration of O_2. At 10% [O_2] (i.e., high [O_2]), hydroxyperoxy radicals are formed via the reaction of O_2 with hydroxyalkyl radicals.

In the squalene reaction, tertiary hydroxyperoxy radicals are the dominant products in the O_2 + hydroxyalkyl radical reaction at 10% [O_2]. Because of the lack of H atoms adjacent to the peroxy radical site in the tertiary hydroxyperoxy radicals, diols and tertiary hydroxyalkoxy radicals are likely the dominant products from the self- and cross-reactions of tertiary hydroxyperoxy radicals. The lack of H atoms adjacent to the peroxy radical site also explains the absence of hydroxycarbonyl products in the squalene GC × GC chromatograms. The tertiary hydroxyalkoxy radicals can subsequently dissociate to form lower molecular weight products. Hydroxyalkoxy radical dissociation is an important channel in the OH + squalene reaction at 10% [O_2], as evident by the large abundance of fragmentation products.

In the linolenic acid reaction, secondary hydroxyperoxy radicals are formed from the O_2 + hydroxyalkyl radical reaction at 10% [O_2]. Hydroxycarbonyl and diol products are the dominant products from the self- and cross-reactions of secondary hydroxyperoxy radicals. Unlike the squalene reaction, the low abundance of fragmentation products indicates that hydroxyalkoxy radicals are likely minor products from the self- and cross-reactions of secondary hydroxyperoxy radicals in the linolenic acid reaction.

dx.doi.org/10.1021/jp508378z | J. Phys. Chem. A 2014, 118, 11555−11571

■ ASSOCIATED CONTENT

Supporting Information

Vacuum ultraviolet mass spectra used for the product identification, quantum chemical calculations of alkoxy radical decomposition, and resonance structures of allylic free radicals. This material is available free of charge via the Internet at http://pubs.acs.org.

■ AUTHOR INFORMATION

Corresponding Author

*(K.R.W.) E-mail: krwilson@lbl.gov.

Notes

The authors declare no competing financial interest.

■ ACKNOWLEDGMENTS

T.N., S.R.L., and K.R.W. are supported by the Director, Office of Energy Research, Office of Basic Energy Sciences, Chemical Sciences Division, of the U.S. Department of Energy under Contract No. DE-AC02-05CH11231. K.R.W. and C.R.R. are additionally supported by the Department of Energy, Office of Science Early Career Research Program. H.Z. is supported by the Camille and Henry Dreyfus foundation postdoctoral program in environmental chemistry. This research used resources of the National Energy Research Scientific Computing Center, which is also supported by the Office of Science of the U.S. Department of Energy under Contract No. DE-AC02-05CH11231.

■ REFERENCES

(1) Rudich, Y. Laboratory Perspectives on the Chemical Transformations of Organic Matter in Atmospheric Particles. *Chem. Rev.* **2003**, *103*, 5097−5124.

(2) Hallquist, M.; Wenger, J. C.; Baltensperger, U.; Rudich, Y.; Simpson, D.; Claeys, M.; Dommen, J.; Donahue, N. M.; George, C.; Goldstein, A. H.; et al. The Formation, Properties and Impact of Secondary Organic Aerosol: Current and Emerging Issues. *Atmos. Chem. Phys.* **2009**, *9*, 5155−5236.

(3) Liu, C. L.; Smith, J. D.; Che, D. L.; Ahmed, M.; Leone, S. R.; Wilson, K. R. The Direct Observation of Secondary Radical Chain Chemistry in the Heterogeneous Reaction of Chlorine Atoms with Submicron Squalane Droplets. *Phys. Chem. Chem. Phys.* **2011**, *13*, 8993−9007.

(4) Ruehl, C. R.; Nah, T.; Isaacman, G.; Worton, D. R.; Chan, A. W. H.; Kolesar, K. R.; Cappa, C. D.; Goldstein, A. H.; Wilson, K. R. The Influence of Molecular Structure and Aerosol Phase on the Heterogeneous Oxidation of Normal and Branched Alkanes by Oh. *J. Phys. Chem. A* **2013**, *117*, 3990−4000.

(5) Renbaum, L. H.; Smith, G. D. The Importance of Phase in the Radical-Initiated Oxidation of Model Organic Aerosols: Reactions of Solid and Liquid Brassidic Acid Particles. *Phys. Chem. Chem. Phys.* **2009**, *11*, 2441−2451.

(6) Renbaum, L. H.; Smith, G. D. Artifacts in Measuring Aerosol Uptake Kinetics: The Roles of Time, Concentration and Adsorption. *Atmos. Chem. Phys.* **2011**, *11*, 6881−6893.

(7) George, I. J.; Abbatt, J. P. D. Heterogeneous Oxidation of Atmospheric Aerosol Particles by Gas-Phase Radicals. *Nat. Chem.* **2010**, *2*, 713−722.

(8) George, I. J.; Vlasenko, A.; Slowik, J. G.; Broekhuizen, K.; Abbatt, J. P. D. Heterogeneous Oxidation of Saturated Organic Aerosols by Hydroxyl Radicals: Uptake Kinetics, Condensed-Phase Products, and Particle Size Change. *Atmos. Chem. Phys.* **2007**, *7*, 4187−4201.

(9) Kessler, S. H.; Smith, J. D.; Che, D. L.; Worsnop, D. R.; Wilson, K. R.; Kroll, J. H. Chemical Sinks of Organic Aerosol: Kinetics and Products of the Heterogeneous Oxidation of Erythritol and Levoglucosan. *Environ. Sci. Technol.* **2010**, *44*, 7005−7010.

(10) Kroll, J. H.; Smith, J. D.; Che, D. L.; Kessler, S. H.; Worsnop, D. R.; Wilson, K. R. Measurement of Fragmentation and Functionalization Pathways in the Heterogeneous Oxidation of Oxidized Organic Aerosol. *Phys. Chem. Chem. Phys.* **2009**, *11*, 8005−8014.

(11) McNeill, V. F.; Yatavelli, R. L. N.; Thornton, J. A.; Stipe, C. B.; Landgrebe, O. Heterogeneous Oh Oxidation of Palmitic Acid in Single Component and Internally Mixed Aerosol Particles: Vaporization and the Role of Particle Phase. *Atmos. Chem. Phys.* **2008**, *8*, 5465−5476.

(12) Smith, J. D.; Kroll, J. H.; Cappa, C. D.; Che, D. L.; Liu, C. L.; Ahmed, M.; Leone, S. R.; Worsnop, D. R.; Wilson, K. R. The Heterogeneous Reaction of Hydroxyl Radicals with Sub-Micron Squalane Particles: A Model System for Understanding the Oxidative Aging of Ambient Aerosols. *Atmos. Chem. Phys.* **2009**, *9*, 3209−3222.

(13) Zhang, H. F.; Ruehl, C. R.; Chan, A. W. H.; Nah, T.; Worton, D. R.; Isaacman, G.; Goldstein, A. H.; Wilson, K. R. Oh-Initiated Heterogeneous Oxidation of Cholestane: A Model System for Understanding the Photochemical Aging of Cyclic Alkane Aerosols. *J. Phys. Chem. A* **2013**, *117*, 12449−12458.

(14) Che, D. L.; Smith, J. D.; Leone, S. R.; Ahmed, M.; Wilson, K. R. Quantifying the Reactive Uptake of Oh by Organic Aerosols in a Continuous Flow Stirred Tank Reactor. *Phys. Chem. Chem. Phys.* **2009**, *11*, 7885−7895.

(15) Wilson, K. R.; Smith, J. D.; Kessler, S. H.; Kroll, J. H. The Statistical Evolution of Multiple Generations of Oxidation Products in the Photochemical Aging of Chemically Reduced Organic Aerosol. *Phys. Chem. Chem. Phys.* **2012**, *14*, 1468−1479.

(16) Atkinson, R. Gas-Phase Tropospheric Chemistry of Organic-Compounds. *J. Phys. Chem. Ref. Data* **1994**, R1−R217.

(17) Atkinson, R. Gas-Phase Tropospheric Chemistry of Volatile Organic Compounds 0.1. Alkanes and Alkenes. *J. Phys. Chem. Ref. Data* **1997**, *26*, 215−290.

(18) Kwok, E. S. C.; Atkinson, R. Estimation of Hydroxyl Radical Reaction-Rate Constants for Gas-Phase Organic-Compounds Using a Structure-Reactivity Relationship - an Update. *Atmos. Environ.* **1995**, *29*, 1685−1695.

(19) Peeters, J.; Boullart, W.; Pultau, V.; Vandenberk, S.; Vereecken, L. Structure-Activity Relationship for the Addition of Oh to (Poly)Alkenes: Site-Specific and Total Rate Constants. *J. Phys. Chem. A* **2007**, *111*, 1618−1631.

(20) Ziemann, P. J.; Atkinson, R. Kinetics, Products, and Mechanisms of Secondary Organic Aerosol Formation. *Chem. Soc. Rev.* **2012**, *41*, 6582−6605.

(21) Atkinson, R.; Arey, J. Atmospheric Degradation of Volatile Organic Compounds. *Chem. Rev.* **2003**, *103*, 4605−4638.

(22) D'andrea, T. M.; Zhang, X.; Jochnowitz, E. B.; Lindeman, T. G.; Simpson, C. J. S. M.; David, D. E.; Curtiss, T. J.; Morris, J. R.; Ellison, G. B. Oxidation of Organic Films by Beams of Hydroxyl Radicals. *J. Phys. Chem. B* **2008**, *112*, 535−544.

(23) Moussa, S. G.; Finlayson-Pitts, B. J. Reaction of Gas Phase Oh with Unsaturated Self-Assembled Monolayers and Relevance to Atmospheric Organic Oxidations. *Phys. Chem. Chem. Phys.* **2010**, *12*, 9419−9428.

(24) Nah, T.; Kessler, S. H.; Daumit, K. E.; Kroll, J. H.; Leone, S. R.; Wilson, K. R. Oh-Initiated Oxidation of Sub-Micron Unsaturated Fatty Acid Particles. *Phys. Chem. Chem. Phys.* **2013**, *15*, 18649−18663.

(25) Nah, T.; Kessler, S. H.; Daumit, K. E.; Kroll, J. H.; Leone, S. R.; Wilson, K. R. Influence of Molecular Structure and Chemical Functionality on the Heterogeneous Oh-Initiated Oxidation of Unsaturated Organic Particles. *J. Phys. Chem. A* **2014**, *118*, 4106−4119.

(26) Kessler, S. H.; Nah, T.; Daumit, K. E.; Smith, J. D.; Leone, S. R.; Kolb, C. E.; Worsnop, D. R.; Wilson, K. R.; Kroll, J. H. Oh-Initiated Heterogeneous Aging of Highly Oxidized Organic Aerosol. *J. Phys. Chem. A* **2012**, *116*, 6358−6365.

(27) Isaacman, G.; Chan, A. W. H.; Nah, T.; Worton, D. R.; Ruehl, C. R.; Wilson, K. R.; Goldstein, A. H. Heterogeneous Oh Oxidation of Motor Oil Particles Causes Selective Depletion of Branched and Less Cyclic Hydrocarbons. *Environ. Sci. Technol.* **2012**, *46*, 10632−10640.

(28) Hearn, J. D.; Renbaum, L. H.; Wang, X.; Smith, G. D. Kinetics and Products from Reaction of Cl Radicals with Dioctyl Sebacate (Dos) Particles in O2: A Model for Radical-Initiated Oxidation of Organic Aerosols. *Phys. Chem. Chem. Phys.* **2007**, *9*, 4803−4813.
(29) Ingold, K. U. Peroxy Radicals. *Acc. Chem. Res.* **1969**, *2*, 1−2.
(30) von Sonntag, C.; Schuchmann, H. P. The Elucidation of Peroxyl Radical Reactions in Aqueous Solution with the Help of Radiation-Chemical Methods. *Angew. Chem., Int. Ed.* **1991**, *30*, 1229−1253.
(31) von Sonntag, C.; Dowideit, P.; Fang, X. W.; Mertens, R.; Pan, X. M.; Schuchmann, M. N.; Schuchmann, H. P. The Fate of Peroxyl Radicals in Aqueous Solution. *Water Sci. Technol.* **1997**, *35*, 9−15.
(32) Bennett, J. E.; Summers, R. Product Studies of Mutual Termination Reactions of Sec-Alkylperoxy Radicals - Evidence for Non-Cyclic Termination. *Can. J. Chem.—Rev. Can. Chim.* **1974**, *52*, 1377−1379.
(33) Atkinson, R.; Tuazon, E. C.; Aschmann, S. M. Products of the Gas-Phase Reaction of the OH Radical with 3-Methyl-1-Butene in the Presence of NO. *Int. J. Chem. Kinet.* **1998**, *30*, 577−587.
(34) Atkinson, R.; Tuazon, E. C.; Carter, W. P. L. Extent of H-Atom Abstraction from the Reaction of the Oh Radical with 1-Butene under Atmospheric Conditions. *Int. J. Chem. Kinet.* **1985**, *17*, 725−734.
(35) Lide, D. R. *CRC Handbook of Chemistry and Physics*, 85th ed.; CRC Pr I Llc: Boca Raton, FL, 2004.
(36) Tesa-Serrate, M. A.; King, K. L.; Paterson, G.; Costen, M. L.; McKendrick, K. G. Site and Bond-Specific Dynamics of Reactions at the Gas-Liquid Interface. *Phys. Chem. Chem. Phys.* **2014**, *16*, 173−183.
(37) Frisch, M. J.; Trucks, G. W.; Schlegel, H. B.; Scuseria, G. E.; Robb, M. A.; Cheeseman, J. R.; Scalmani, G.; Barone, V.; Mennucci, B.; Petersson, G. A., et al., *Gaussian 09, Revision D.01*;, Gaussian, Inc.: Wallingford CT, 2009.
(38) Khursan, S. L.; Martem'yanov, V. S.; Denisov, E. T. Mechanism of the Recombination of Peroxyl Radicals. *Kinet. Catal.* **1989**, *31*, 1031−1040.
(39) Bennett, J. E.; Brunton, G.; Smith, J. R. L.; Salmon, T. M. F.; Waddington, D. J. Reactions of Alkylperoxyl Radicals in Solution 0.1. A Kinetic-Study of Self-Reactions of 2-Propylperoxyl Radicals between 135-K and 300-K. *J. Chem. Soc. Faraday Trans.* **1987**, *83*, 2421−2432.
(40) Denisov, E. T.; Afanas'ev, I. B. *Oxidation and Antioxidants in Organic Chemistry and Biology*. CRC Press: Boca Raton, FL, 2005.
(41) Hearn, J. D.; Lovett, A. J.; Smith, G. D. Ozonolysis of Oleic Acid Particles: Evidence for a Surface Reaction and Secondary Reactions Involving Criegee Intermediates. *Phys. Chem. Chem. Phys.* **2005**, *7*, 501−511.
(42) Docherty, K. S.; Ziemann, P. J. Reaction of Oleic Acid Particles with No3 Radicals: Products, Mechanism, and Implications for Radical-Initiated Organic Aerosol Oxidation. *J. Phys. Chem. A* **2006**, *110*, 3567−3577.